

# A Belief Propagation Algorithm for Multipath-Based SLAM

Erik Leitinger, *Member, IEEE*, Florian Meyer, *Member, IEEE*, Franz Hlawatsch, *Fellow, IEEE*, Klaus Witrisal, *Member, IEEE*, Fredrik Tufvesson, *Fellow, IEEE*, and Moe Z. Win, *Fellow, IEEE*

## Abstract

We present a simultaneous localization and mapping (SLAM) algorithm that is based on radio signals and the association of specular multipath components (MPCs) with geometric features. Especially in indoor scenarios, *robust* localization from radio signals is challenging due to diffuse multipath propagation, unknown MPC-feature association, and limited visibility of features. In our approach, specular reflections at flat surfaces are described in terms of virtual anchors (VAs) that are mirror images of the physical anchors (PAs). The positions of these VAs and possibly also of the PAs are unknown. We develop a Bayesian model of the SLAM problem including the unknown MPC-VA/PA association. We represent this model by a factor graph, which enables the use of the belief propagation (BP) scheme for efficient marginalization of the joint posterior distribution. The resulting BP-based SLAM algorithm detects the VAs associated with the PAs and estimates jointly the time-varying position of the mobile agent and the positions of the VAs and possibly also of the PAs, thereby leveraging the MPCs in the radio signal for improved accuracy and robustness of agent localization. A core aspect of the algorithm is BP-based probabilistic MPC-VA/PA association. Moreover, for improved initialization of new VA positions, the states of unobserved potential VAs are modeled as a random finite set and propagated in time by means of a “zero-measurement” probability hypothesis density filter. The proposed BP-based SLAM algorithm has a low computational complexity and scales well in all relevant system parameters. Experimental results using both synthetically generated measurements and real ultra-wideband radio signals demonstrate the excellent performance of the algorithm in challenging indoor environments.

## Index Terms

Simultaneous localization and mapping, SLAM, multipath channel, data association, factor graph, message passing, sum-product algorithm.

E. Leitinger and F. Tufvesson are with the Department of Electrical and Information Technology, Lund University, Lund, Sweden (e-mail: {erik.leitinger, fredrik.tufvesson}@eit.lth.se). F. Meyer and M. Win are with the Laboratory for Information and Decision Systems, Massachusetts Institute of Technology, Cambridge, MA, USA (e-mail: {fmeyer, moewin}@mit.edu). F. Hlawatsch is with the Institute of Telecommunications, TU Wien, Vienna, Austria and with Brno University of Technology, Brno, Czech Republic (e-mail: franz.hlawatsch@tuwien.ac.at). K. Witrisal is with the Christian Doppler Laboratory for location-aware electronic systems, Graz University of Technology, Graz, Austria, (e-mail: witrisal@tugraz.at). This work was supported in part by the Austrian Science Fund (FWF) under grants J 4027, J 3886, and P27370-N30, by the U.S. Department of Commerce, National Institute of Standards and Technology under Grant 70NANB17H17, and by the Czech Science Foundation (GAČR) under grant 17-19638S. Parts of this paper were presented at IEEE ICC, ANLN Workshop 2017, Paris, France, June 2017.

## I. INTRODUCTION

The purpose of simultaneous localization and mapping (SLAM) [1] is to estimate the time-varying pose of a mobile agent—which includes the agent’s position—and a map of the surrounding environment, from measurements provided by one or multiple sensors. SLAM has attracted strong interest in robotics research for many years. Other fields that rely on accurate localization and environment mapping include autonomous driving [2], location-aware communication [3], and robust indoor localization [4]–[7]. Achieving a required level of accuracy robustly is still elusive in indoor environments characterized by harsh multipath channel conditions. Therefore, most existing systems supporting multipath channels either use sensing technologies that mitigate multipath effects [8] or fuse information from multiple information sources [9].

In multipath-assisted indoor localization [4], [10], [11], multipath components (MPCs) are related to the local geometry. This potentially turns multipath propagation from an impairment into an advantage. This paper presents a SLAM algorithm for robust indoor localization based on radio signals. In our setup, the radio signals are transmitted from a mobile agent to base stations, called physical anchors (PAs). MPCs due to specular reflections at flat surfaces are modeled by virtual anchors (VAs), which are mirror images of the PAs [12]. Our proposed algorithm is able to detect the VAs associated with the PAs and to accurately estimate the VA positions and possibly also the PA positions jointly with the time-varying position of the mobile agent. Our algorithm is designed to cope with measurements obtained from radio signals under harsh multipath channel conditions, i.e., measurements with a high level of false alarms and missed detections. While MPCs can be generated by various propagation phenomena such as specular reflections, scattering, and diffraction, our model focuses on PA/VA-related MPCs; all the other MPCs are treated as interference, even if they contain geometric information. We note that MPCs associated with scatter points are also considered in the feature model used in [10].

### A. Feature-based SLAM

The proposed algorithm follows the feature-based approach to SLAM [1], [13], [14]. The map is represented by an unknown number of *features* with unknown spatial positions, whose states are estimated in a sequential (time-recursive) way. Features are parametric descriptions of the physical environment such as flat surfaces, edges, corners, points, or circles. In our model, the features are given by the PAs and VAs. Prominent feature-based SLAM algorithms are extended Kalman filter SLAM (EKF-SLAM) [13], Rao-Blackwellized SLAM (dubbed Fast-

SLAM) [1], [15], variational-inference-based SLAM [16], [17], and set-based SLAM [14], [18], [19]. Recently, feature-based SLAM methods that exploit position-related information in radio signals were introduced [10], [20], [21]. Most of these methods operate on estimated parameters related to MPCs, such as distances (which are proportional to delays), angles-of-arrival (AoAs), or angles-of-departure (AoDs) [22]–[26]. These parameters are estimated from the signal in a preprocessing stage and are considered as “measurements” by the SLAM method. An important aspect is the *data association* (DA) between these measurements and the PAs or VAs. For simplicity, we assume time synchronization between the PAs and the mobile agent. However, the proposed algorithm can be extended to nonsynchronized PA-agent links along the lines of [10] (based on the fact that the relevant geometric information is also contained in the time differences of the MPCs [11]) or to joint SLAM and synchronization along the lines of [27].

Feature-based SLAM is closely related to the multitarget tracking (MTT) problem, and consequently MTT methods have been adapted to feature-based SLAM [14], [18], [28]. MTT methods that are applicable to SLAM include the joint probabilistic DA (JPDA) filter [29] and the joint integrated probabilistic DA (JIPDA) filter [30]. An approach similar to the JIPDA filter is taken by the methods presented in [31], [32], which determine a track quality measure and use an additional random finite set (RFS)-based probability hypothesis density (PHD) filter [33] to initialize new objects. More recently, the use of the belief propagation (BP) message passing scheme [34], [35] was introduced for probabilistic DA within MTT in [36] and for multisensor MTT in [37]–[40]. In particular, the BP algorithms in [38]–[41] are based on a factor graph representation of the multisensor MTT problem and have a computational complexity that scales only quadratically with the number of objects (targets) and linearly with the number of sensors. MTT methods that are based on RFSs and embed a BP algorithm for probabilistic DA were presented in [42], [43]. We finally note that our approach to feature-based SLAM is also related to multisensor target tracking with uncertain sensor locations using Bayesian methods [44].

## B. Contributions and Organization of the Paper

Here, we propose a BP algorithm for SLAM based on radio signals. The algorithm jointly performs probabilistic DA and sequential Bayesian estimation of the state of a mobile agent and the states of “potential features” (PFs) characterizing the environment. Each PF state is augmented by a binary existence variable and associated with a *probability of existence*, which is also estimated. The proposed SLAM algorithm is inspired by the BP algorithms for multisensor

MTT presented in [38]–[40]. Probabilistic DA and state estimation are performed by running BP on a factor graph [34], [35] representing the statistical structure of the SLAM detection-estimation problem. The BP approach leverages conditional statistical independencies to achieve low complexity and high scalability. Indeed, our algorithm inherits the excellent scalability of the MTT algorithms presented in [37], [38]: its complexity scales only quadratically with the numbers of features and measurements and linearly with the number of PAs. A major reason for this scalability is the integration of the BP-based probabilistic DA scheme from [36], [38]. The proposed algorithm distinguishes between *legacy PFs*, which correspond to features that already generated measurements in the past, and *new PFs*, which correspond to features that generate measurements for the first time. The parameters required to initialize new PFs are modeled explicitly by means of an *undetected feature* state and inferred using a “zero-measurement” PHD filter, which was introduced in the context of MTT in [32], [42]. To the best of our knowledge, the proposed algorithm—along with a preliminary version presented in [28]—is the first BP algorithm for feature-based SLAM with probabilistic DA.

Key innovative contributions of this paper include the following:

- We develop a BP algorithm for feature-based SLAM with probabilistic DA that uses MPC parameters extracted from radio signals as input measurements. The algorithm takes into account that the number of features is unknown and possibly time-varying, and it scales well with all relevant system parameters.
- We consider the states of *new PFs* and an *undetected feature* state. The intensity function of the undetected feature state is tracked by a zero-measurement PHD filter [32]. The estimated intensity function is used to determine the initial distribution of new PFs.
- We evaluate the performance of the proposed algorithm on synthetic and real data. Our results show that the algorithm is able to estimate the position of the mobile agent and a possibly time-varying feature map with high accuracy and robustness.

We apply the proposed algorithm to the challenging setup of a range-only measurement model. However, bearing information (AoA and AoD of MPCs) or information derived from inertial measurement unit sensors can be easily incorporated in the measurement and state-evolution models underlying our algorithm, and this would lead to a significant performance gain.

This paper advances over our conference paper [28] in that it replaces the heuristic used therein for determining the initial distribution of new PFs by an improved Bayesian scheme. The factor graph and BP algorithm of [28] are extended by the introduction of new PFs, i.e., features that

generate measurements for the first time. For simplicity, we assume that the probabilities with which the preliminary signal analysis stage (producing measurements) detects features in the radio signals are known; however, an adaptive extension to unknown and time-varying detection probabilities can be obtained along the lines of [28], [39], [45].

The remainder of this paper is organized as follows. Section II considers the received radio signals and the MPC parameters. Section III describes the system model and provides a statistical formulation of the SLAM problem. The posterior distribution of all states and the corresponding factor graph are derived in Section IV. In Section V, the proposed BP algorithm is described. Section VI discusses the determination of the initial distribution of new PFs. The results of numerical experiments are reported in Section VII. Section VIII concludes the paper.

## II. RADIO SIGNAL AND MPC PARAMETERS

Radio signal based SLAM [4], [10], [20], [21] exploits position-related information in MPCs [11]. Specular MPC parameters estimated from the received radio signals are associated with “geometrically expected” parameters, such as distances (corresponding to delays), AoAs, and AoDs. These “geometrically expected” parameters are modeled in terms of the position of the mobile agent and the positions of the PAs or of the corresponding VAs. The VA positions are mirror images of the PA positions. These mirror images are induced by reflections at flat surfaces (typically walls), and thus depend on the surrounding environment (floor plan) [12]. For each reflection path, the length from the PA (via the flat surface) to the mobile agent is equal to the length from the VA to the mobile agent. Even though the mobile agent moves, the VAs remain static as long as the PAs and flat surfaces (floor plan) are static. Note that the VA positions are unknown because the floor plan is unknown. An example is shown in Fig. 1, which depicts two PAs and some of the corresponding first-order VAs belonging to some larger flat surfaces. Also shown are two reflection paths (for the two PAs) for mobile agent position  $\mathbf{p}_{350}$ .

We consider a mobile agent with unknown time-varying position  $\mathbf{p}_n \in \mathbb{R}^2$  and  $J$  PAs with possibly unknown positions  $\mathbf{a}_{1,n}^{(j)} \in \mathbb{R}^2$ ,  $j = 1, \dots, J$ , where  $J$  is assumed to be known. Associated with the  $j$ th PA, there are  $L_n^{(j)} - 1$  VAs at unknown and possibly time-varying positions  $\mathbf{a}_{l,n}^{(j)} \in \mathbb{R}^2$ ,  $l = 2, \dots, L_n^{(j)}$ . The PAs and VAs will also be referred to as *features*. The number of features,  $L_n^{(j)}$ , is unknown and time-varying, and it depends on the agent position  $\mathbf{p}_n$ . We note that the PA and VA positions are allowed to be time-varying for the sake of generality; in an indoor scenario, they are typically static. In each discrete time slot  $n$ , the mobile agent transmits a radio signal

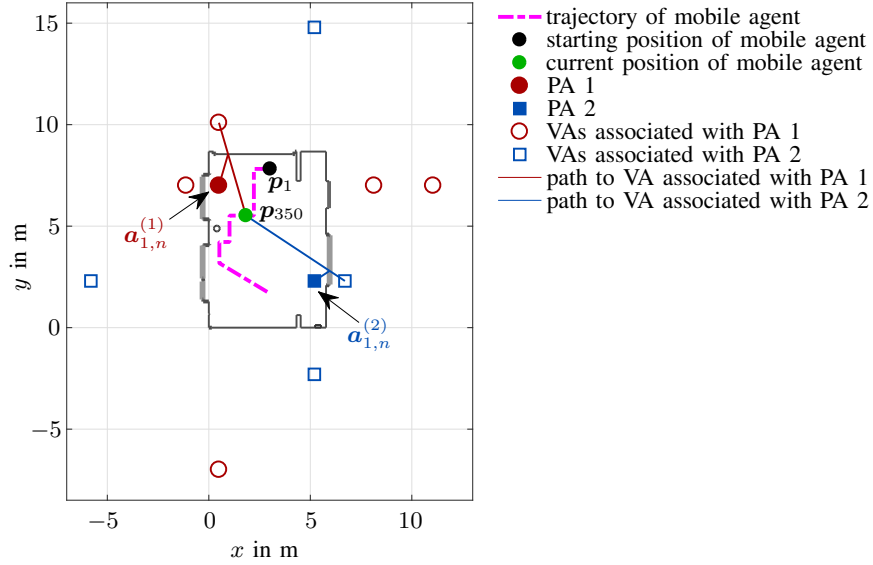


Fig. 1: Example of an environment map (floor plan). The PAs at fixed positions  $\mathbf{a}_{1,n}^{(1)}$  (PA 1) and  $\mathbf{a}_{1,n}^{(2)}$  (PA 2) are indicated by, respectively, a red bullet and a blue box within the floor plan. The magenta dashed-dotted line represents the trajectory of the mobile agent. The starting position of the mobile agent,  $\mathbf{p}_1$ , and the position  $\mathbf{p}_{350}$  (at discrete time  $n=350$ ) are indicated by a black and a green bullet, respectively. The red circles and blue squares outside the floor plan indicate some of the geometrically expected VAs associated with PA 1 and PA 2, respectively. Two exemplary reflection paths between the mobile agent at position  $\mathbf{p}_{350}$  and two VAs associated with the two PAs are shown by red and blue lines.

$s(t)$  and the PAs act as receivers. However the proposed algorithm can be easily reformulated for the case where the PAs act as transmitters and the mobile agent acts as a receiver.

The baseband signal received by the  $j$ th PA is modeled as [11]

$$r_n^{(j)}(t) = \sum_{l=1}^{L_n^{(j)}} \alpha_{l,n}^{(j)} s(t - \tau_{l,n}^{(j)}) + d_n^{(j)}(t) + w(t). \quad (1)$$

Here, the first term on the right-hand side describes the contribution of  $L_n^{(j)}$  specular MPCs with complex amplitudes  $\alpha_{l,n}^{(j)}$  and delays  $\tau_{l,n}^{(j)}$ , where  $l \in \mathcal{L}_n^{(j)} \triangleq \{1, \dots, L_n^{(j)}\}$ . The specular MPCs potentially correspond to features (PAs or VAs). The delays  $\tau_{l,n}^{(j)}$  are proportional to the distances (ranges) between the agent and the  $j$ th PA (for  $l=1$ ) or between the agent and the VAs associated with the  $j$ th PA (for  $l \in \{2, \dots, L_n^{(j)}\}$ ). That is,  $\tau_{l,n}^{(j)} = \|\mathbf{p}_n - \mathbf{a}_{l,n}^{(j)}\|/c$ , where  $c$  is the speed of light. The second term in (1),  $d_n^{(j)}(t)$ , represents the diffuse multipath, which shares the same spectrum as  $s(t)$  and interferes with the position-related MPC term. The third and last term in (1),  $w(t)$ , is additive white Gaussian noise. We note that expression (1) presupposes a common time reference at the mobile agent and at the PAs, i.e., a synchronized system. However, the proposed

SLAM algorithm can be extended to the unsynchronized case along the lines discussed in [10], exploiting the fact that the geometric information contained in the MPC delays is preserved in the time differences of the MPC delays [11]. Furthermore, our algorithm can also be extended to the case where the MPC parameters include AoAs and/or AoDs in addition to the delays  $\tau_{l,n}^{(j)}$ . An extension of our algorithm that uses the complex MPC amplitudes to directly estimate the detection probability of each feature has been proposed in [45].

In each time slot  $n$  and for each PA  $j \in \{1, \dots, J\}$ , the MPC parameters (e.g., delays, AoAs, and AoDs) are estimated from the radio signals  $r_n^{(j)}(t)$  using a snapshot-based [22], [23], [25], [26] or state space-based [24], [46] parametric radio channel estimator. This results in  $M_n^{(j)}$  estimates of MPC parameters along with estimates of the corresponding complex amplitudes  $\hat{\alpha}_{m,n}^{(j)}$ , with  $m \in \mathcal{M}_n^{(j)} \triangleq \{1, \dots, M_n^{(j)}\}$ , for each PA  $j \in \{1, \dots, J\}$ . The set of estimated MPC parameters  $\mathcal{M}_n^{(j)}$  is related to the set of specular MPCs  $\mathcal{L}_n^{(j)}$  as follows. It is possible that some specular MPCs are not “detected” by the radio channel estimator and thus do not produce an MPC parameter estimate, and it is also possible that some estimates do not correspond to specular MPCs. Accordingly,  $M_n^{(j)} = |\mathcal{M}_n^{(j)}|$  may be smaller than, equal to, or larger than  $L_n^{(j)} = |\mathcal{L}_n^{(j)}|$ . (Here,  $|\cdot|$  denotes the cardinality of a set.) Note also that  $M_n^{(j)}$  depends on the agent position  $\mathbf{p}_n$ , on the surrounding environment, and on the channel parameter estimation algorithm. The amplitude estimates are used to determine estimates of the MPC parameter variances  $\hat{\sigma}_{m,n}^{(j)2}$ , if such variance estimates are not provided by the channel estimator (cf. Section VII-C). We denote by  $\mathbf{z}_{m,n}^{(j)}$  with  $m \in \mathcal{M}_n^{(j)}$  the estimated parameters of the  $m$ th MPC of PA  $j$ . The stacked vectors  $\mathbf{z}_n^{(j)} \triangleq [\mathbf{z}_{1,n}^{(j)\top} \cdots \mathbf{z}_{M_n^{(j)},n}^{(j)\top}]^\top$  are used as noisy “measurements” by the proposed SLAM algorithm.

### III. SYSTEM MODEL AND STATISTICAL FORMULATION

#### A. Agent State and PF States

The state of the mobile agent at time  $n$  is defined as  $\mathbf{x}_n \triangleq [\mathbf{p}_n^\top \mathbf{v}_n^\top]^\top$ , where  $\mathbf{v}_n$  is the agent’s velocity. For each PA  $j \in \{1, \dots, J\}$ , there are  $K_n^{(j)}$  PFs. Thus, the PFs will be indexed by the tuple  $(j, k)$ , where  $j \in \{1, \dots, J\}$  and  $k \in \mathcal{K}_n^{(j)} \triangleq \{1, \dots, K_n^{(j)}\}$ . Whereas the number of PAs  $J$  is known, the number of PFs  $K_n^{(j)}$  (for PA  $j$ ) is unknown and random. The existence of the  $(j, k)$ th PF as an actual *feature* is indicated by the binary existence variable  $r_{k,n}^{(j)} \in \{0, 1\}$ , where  $r_{k,n}^{(j)} = 0$  ( $r_{k,n}^{(j)} = 1$ ) means that the PF does not exist (exists) at time  $n$ . The state of PF  $(j, k)$  is the PF’s position  $\mathbf{a}_{k,n}^{(j)}$ , and the *augmented state* of a PF  $(j, k)$  is defined as  $\mathbf{y}_{k,n}^{(j)} \triangleq [\mathbf{a}_{k,n}^{(j)\top} r_{k,n}^{(j)}]^\top$  [38]. We also define the stacked vectors  $\mathbf{y}_n^{(j)} \triangleq [\mathbf{y}_{1,n}^{(j)\top} \cdots \mathbf{y}_{K_n^{(j)},n}^{(j)\top}]^\top$  and  $\mathbf{y}_n \triangleq [\mathbf{y}_n^{(1)\top} \cdots \mathbf{y}_n^{(J)\top}]^\top$ . It will be

convenient to formally consider PF states also for the nonexisting PFs (case  $r_{k,n}^{(j)} = 0$ ); however, the values of these states are obviously irrelevant. Therefore, all probability density functions (pdfs) defined for an augmented state,  $f(\mathbf{y}_{k,n}) = f(\mathbf{a}_{k,n}^{(j)}, r_{k,n}^{(j)})$ , are such that for  $r_{k,n}^{(j)} = 0$ ,  $f(\mathbf{a}_{k,n}^{(j)}, 0) = f_{k,n}^{(j)} f_D(\mathbf{a}_{k,n}^{(j)})$ , where  $f_D(\mathbf{a}_{k,n}^{(j)})$  is an arbitrary ‘‘dummy pdf’’ and  $f_{k,n}^{(j)} \geq 0$  can be interpreted as the probability of nonexistence of the PF [38]. We note that the joint augmented PF state, described here by the random vector  $\mathbf{y}_n^{(j)}$ , could be alternatively modeled by a multi-Bernoulli random finite set, similarly to [42]. However, the unordered nature of random finite sets would complicate the development of a factor graph and a BP algorithm.

At any time  $n$ , each PF is either a *legacy PF*, which was already established in the past, or a *new PF*, which is established for the first time. The augmented states of legacy PFs and new PFs for PA  $j$  will be denoted by  $\tilde{\mathbf{y}}_{k,n}^{(j)} \triangleq [\tilde{\mathbf{a}}_{k,n}^{(j)\text{T}} \tilde{r}_{k,n}^{(j)}]^\text{T}$ ,  $k \in \mathcal{K}_{n-1}^{(j)}$  and  $\check{\mathbf{y}}_{m,n}^{(j)} \triangleq [\check{\mathbf{a}}_{m,n}^{(j)\text{T}} \check{r}_{m,n}^{(j)}]^\text{T}$ ,  $m \in \mathcal{M}_n^{(j)}$ , respectively. Thus, the number of new PFs equals the number of measurements,  $M_n^{(j)}$ . The set and number of legacy PFs are updated according to

$$\mathcal{K}_n^{(j)} = \mathcal{K}_{n-1}^{(j)} \cup \mathcal{M}_n^{(j)}, \quad K_n^{(j)} = K_{n-1}^{(j)} + M_n^{(j)}, \quad (2)$$

where the first relation is understood to include a suitable reindexing of the elements of  $\mathcal{M}_n^{(j)}$ . (The number of PFs does not actually grow by  $M_n^{(j)}$  because the set of PFs is pruned as explained in Section V-A.) We also define the following state-related vectors. For the legacy PFs for PA  $j$ ,  $\tilde{\mathbf{a}}_n^{(j)} \triangleq [\tilde{\mathbf{a}}_{1,n}^{(j)\text{T}} \cdots \tilde{\mathbf{a}}_{K_{n-1}^{(j)},n}^{(j)\text{T}}]^\text{T}$ ,  $\tilde{\mathbf{r}}_n^{(j)} \triangleq [\tilde{r}_{1,n}^{(j)} \cdots \tilde{r}_{K_{n-1}^{(j)},n}^{(j)}]^\text{T}$ , and  $\tilde{\mathbf{y}}_n^{(j)} \triangleq [\tilde{\mathbf{y}}_{1,n}^{(j)\text{T}} \cdots \tilde{\mathbf{y}}_{K_{n-1}^{(j)},n}^{(j)\text{T}}]^\text{T}$ . For the new PFs for PA  $j$ ,  $\check{\mathbf{a}}_n^{(j)} \triangleq [\check{\mathbf{a}}_{1,n}^{(j)\text{T}} \cdots \check{\mathbf{a}}_{M_n^{(j)},n}^{(j)\text{T}}]^\text{T}$ ,  $\check{\mathbf{r}}_n^{(j)} \triangleq [\check{r}_{1,n}^{(j)} \cdots \check{r}_{M_n^{(j)},n}^{(j)}]^\text{T}$ , and  $\check{\mathbf{y}}_n^{(j)} \triangleq [\check{\mathbf{y}}_{1,n}^{(j)\text{T}} \cdots \check{\mathbf{y}}_{M_n^{(j)},n}^{(j)\text{T}}]^\text{T}$ . For the combination of legacy PFs and new PFs for PA  $j$ ,  $\mathbf{y}_n^{(j)} \triangleq [\tilde{\mathbf{y}}_n^{(j)\text{T}} \check{\mathbf{y}}_n^{(j)\text{T}}]^\text{T}$ ; note that the vector entries (subvectors) of  $\mathbf{y}_n^{(j)}$  are given by  $\mathbf{y}_{k,n}^{(j)}$  for  $k \in \mathcal{K}_n^{(j)} = \mathcal{K}_{n-1}^{(j)} \cup \mathcal{M}_n^{(j)}$ . For all the legacy PFs,  $\tilde{\mathbf{y}}_n \triangleq [\tilde{\mathbf{y}}_n^{(1)\text{T}} \cdots \tilde{\mathbf{y}}_n^{(J)\text{T}}]^\text{T}$ , and for all the new PFs,  $\check{\mathbf{y}}_n \triangleq [\check{\mathbf{y}}_n^{(1)\text{T}} \cdots \check{\mathbf{y}}_n^{(J)\text{T}}]^\text{T}$ .

The number of new PFs at time  $n$  is known only after the current measurements have been observed. Features that are observed for the first time will be referred to as *newly detected features*. Before the current measurements are observed, only prior information is available about the newly detected features (as discussed in Section VI-B). After the current measurements are observed, newly detected features are represented by new PFs.

## B. Association Vectors

For each PA  $j$ , the measurements (MPC parameter estimates)  $\mathbf{z}_{m,n}^{(j)}$ ,  $m \in \mathcal{M}_n^{(j)}$  described in Section II are subject to a measurement origin uncertainty, also known as DA uncertainty.

That is, it is not known which measurement  $\mathbf{z}_{m,n}^{(j)}$  is associated with which PF  $k \in \mathcal{K}_n^{(j)}$ , or if a measurement  $\mathbf{z}_{m,n}^{(j)}$  did not originate from any PF (this is known as a *false alarm* or *clutter*), or if a PF did not give rise to any measurement (this is known as a *missed detection*). The probability that a PF is “detected” in the sense that it generates a measurement  $\mathbf{z}_{m,n}^{(j)}$  in the MPC parameter estimation stage is denoted by  $P_d^{(j)}(\mathbf{x}_n, \mathbf{a}_{k,n}^{(j)})$ . The distribution of false alarm measurements is described by the pdf  $f_{\text{FA}}(\mathbf{z}_{m,n}^{(j)})$ . The functions  $P_d^{(j)}(\mathbf{x}_n, \mathbf{a}_{k,n}^{(j)}) \in (0, 1]$  and  $f_{\text{FA}}(\mathbf{z}_{m,n}^{(j)}) \geq 0$  are assumed known. Following [29], we assume that at any time  $n$ , each PF can generate at most one measurement, and each measurement can be generated by at most one PF.

For each PA  $j$ , the associations between the measurements  $m \in \mathcal{M}_n^{(j)}$  and the legacy PF states  $(j, k)$ ,  $k \in \mathcal{K}_{n-1}^{(j)}$  at time  $n$  can be described by the  $K_{n-1}^{(j)}$ -dimensional *feature-oriented DA vector*  $\mathbf{c}_n^{(j)} = [c_{1,n}^{(j)} \cdots c_{K_{n-1}^{(j)},n}^{(j)}]^\top$  with entries

$$c_{k,n}^{(j)} \triangleq \begin{cases} m \in \mathcal{M}_n^{(j)}, & \text{if at time } n, \text{ legacy PF } (j, k) \text{ generates measurement } \mathbf{z}_{m,n}^{(j)}; \\ 0, & \text{if at time } n, \text{ legacy PF } (j, k) \text{ does not generate any measurement.} \end{cases} \quad (3)$$

We also define  $\mathbf{c}_n \triangleq [\mathbf{c}_n^{(1)\top} \cdots \mathbf{c}_n^{(J)\top}]^\top$ . In addition, following [36], [38], we consider the  $M_n^{(j)}$ -dimensional *measurement-oriented DA vector*  $\mathbf{b}_n^{(j)} = [b_{1,n}^{(j)} \cdots b_{M_n^{(j)},n}^{(j)}]^\top$  with entries

$$b_{m,n}^{(j)} \triangleq \begin{cases} k \in \mathcal{K}_{n-1}^{(j)}, & \text{if measurement } \mathbf{z}_{m,n}^{(j)} \text{ is generated by legacy PF } (j, k); \\ 0, & \text{if measurement } \mathbf{z}_{m,n}^{(j)} \text{ is not generated by any legacy PF.} \end{cases} \quad (4)$$

We also define  $\mathbf{b}_n \triangleq [\mathbf{b}_n^{(1)\top} \cdots \mathbf{b}_n^{(J)\top}]^\top$ . The two DA vectors  $\mathbf{c}_n$  and  $\mathbf{b}_n$  are unknown and modeled as random. They are equivalent since one can be determined from the other. The redundant formulation of DA uncertainty in terms of both  $\mathbf{c}_n$  and  $\mathbf{b}_n$  is key to obtaining the scalability properties of the BP algorithm to be presented in Section V-B. Furthermore, as will be discussed in Section IV, it facilitates the establishment of a factor graph for the problem of jointly inferring the agent state and the states of the legacy PFs and new PFs.

### C. State Evolution

The agent state  $\mathbf{x}_n$  and the augmented states of the legacy PFs,  $\tilde{\mathbf{y}}_{k,n}^{(j)}$ , are assumed to evolve independently according to Markovian state dynamics, i.e.,

$$f(\mathbf{x}_n, \tilde{\mathbf{y}}_n | \mathbf{x}_{n-1}, \mathbf{y}_{n-1}) = f(\mathbf{x}_n | \mathbf{x}_{n-1}) f(\tilde{\mathbf{y}}_n | \mathbf{y}_{n-1}) = f(\mathbf{x}_n | \mathbf{x}_{n-1}) \prod_{j=1}^J \prod_{k=1}^{K_{n-1}^{(j)}} f(\tilde{\mathbf{y}}_{k,n}^{(j)} | \mathbf{y}_{k,n-1}^{(j)}), \quad (5)$$

where  $f(\mathbf{x}_n | \mathbf{x}_{n-1})$  and  $f(\tilde{\mathbf{y}}_{k,n}^{(j)} | \mathbf{y}_{k,n-1}^{(j)})$  are the state-transition pdfs of the agent and of legacy PF

$(j, k)$ , respectively. Note that  $\tilde{\mathbf{y}}_{k,n}^{(j)}$  depends on both  $\tilde{\mathbf{y}}_{k,n-1}^{(j)}$  and  $\check{\mathbf{y}}_{m,n-1}^{(j)}$ . If PF  $(j, k)$  exists at time  $n-1$ , i.e.,  $r_{k,n-1}^{(j)} = 1$ , it either dies, i.e.,  $\tilde{r}_{k,n}^{(j)} = 0$ , or survives, i.e.,  $\tilde{r}_{k,n}^{(j)} = 1$ ; in the latter case, it becomes a legacy PF at time  $n$ . The probability of survival is denoted by  $P_s$ . If the PF survives, its new state  $\tilde{\mathbf{a}}_{k,n}^{(j)}$  is distributed according to the state-transition pdf  $f(\tilde{\mathbf{a}}_{k,n}^{(j)} | \mathbf{a}_{k,n-1}^{(j)})$ . Therefore,  $f(\tilde{\mathbf{y}}_{k,n}^{(j)} | \mathbf{y}_{k,n-1}^{(j)}) = f(\tilde{\mathbf{a}}_{k,n}^{(j)}, \tilde{r}_{k,n}^{(j)} | \mathbf{a}_{k,n-1}^{(j)}, r_{k,n-1}^{(j)})$  in (5) is given for  $r_{k,n-1}^{(j)} = 1$  by

$$f(\tilde{\mathbf{a}}_{k,n}^{(j)}, \tilde{r}_{k,n}^{(j)} | \mathbf{a}_{k,n-1}^{(j)}, r_{k,n-1}^{(j)} = 1) = \begin{cases} (1 - P_s) f_D(\tilde{\mathbf{a}}_{k,n}^{(j)}), & \tilde{r}_{k,n}^{(j)} = 0 \\ P_s f(\tilde{\mathbf{a}}_{k,n}^{(j)} | \mathbf{a}_{k,n-1}^{(j)}), & \tilde{r}_{k,n}^{(j)} = 1. \end{cases} \quad (6)$$

If PF  $(j, k)$  does not exist at time  $n-1$ , i.e.,  $r_{k,n-1}^{(j)} = 0$ , it cannot exist as a legacy PF at time  $n$  either. Therefore,

$$f(\tilde{\mathbf{a}}_{k,n}^{(j)}, \tilde{r}_{k,n}^{(j)} | \mathbf{a}_{k,n-1}^{(j)}, r_{k,n-1}^{(j)} = 0) = \begin{cases} f_D(\tilde{\mathbf{a}}_{k,n}^{(j)}), & \tilde{r}_{k,n}^{(j)} = 0 \\ 0, & \tilde{r}_{k,n}^{(j)} = 1. \end{cases} \quad (7)$$

#### D. Prior Distributions

For a given PA  $j$ , there are  $M_n^{(j)} = |\mathcal{M}_n^{(j)}|$  new PFs at time  $n$ . The number of false alarms is assumed Poisson distributed with mean  $\mu_{\text{FA}}^{(j)}$  [29], [47]. Similarly, the number of newly detected features is assumed Poisson distributed with mean  $\mu_{n,n}^{(j)}$ ; the calculation of  $\mu_{n,n}^{(j)}$  will be discussed in Section VI. Then, one can derive the following expression of the joint conditional prior probability mass function (pmf) of the DA vector  $\mathbf{c}_n^{(j)}$ , the vector of existence indicators of new PFs,  $\check{\mathbf{r}}_n^{(j)}$ , and the number of measurements or equivalently new PFs,  $M_n^{(j)}$ , given the state of the mobile agent,  $\mathbf{x}_n$ , and the vector of augmented states of legacy PFs,  $\tilde{\mathbf{y}}_n^{(j)}$  (cf. [38])

$$p(\mathbf{c}_n^{(j)}, \check{\mathbf{r}}_n^{(j)}, M_n^{(j)} | \mathbf{x}_n, \tilde{\mathbf{y}}_n^{(j)}) = \chi_{\mathbf{c}_n^{(j)}, \check{\mathbf{r}}_n^{(j)}, M_n^{(j)}} \psi(\mathbf{c}_n^{(j)}) \left( \prod_{m \in \mathcal{N}_{\check{\mathbf{r}}_n^{(j)}}^{(j)}} \Gamma_{\mathbf{c}_n^{(j)}}(\check{r}_{m,n}^{(j)}) \right) \left( \prod_{k \in \mathcal{D}_{\mathbf{c}_n^{(j)}, \check{\mathbf{r}}_n^{(j)}}^{(j)}} P_d^{(j)}(\mathbf{x}_n, \mathbf{a}_{k,n}^{(j)}) \right) \\ \times \prod_{k' \in \bar{\mathcal{D}}_{\mathbf{c}_n^{(j)}, \check{\mathbf{r}}_n^{(j)}}^{(j)}} [1 - \tilde{r}_{k',n}^{(j)} P_d^{(j)}(\mathbf{x}_n, \tilde{\mathbf{a}}_{k',n}^{(j)})], \quad (8)$$

with  $\chi_{\mathbf{c}_n^{(j)}, \check{\mathbf{r}}_n^{(j)}, M_n^{(j)}} \triangleq e^{-(\mu_{\text{FA}}^{(j)} + \mu_{n,n}^{(j)})} (\mu_{n,n}^{(j)})^{|\mathcal{N}_{\check{\mathbf{r}}_n^{(j)}}^{(j)}|} (\mu_{\text{FA}}^{(j)})^{M_n^{(j)} - |\mathcal{D}_{\mathbf{c}_n^{(j)}, \check{\mathbf{r}}_n^{(j)}}^{(j)}| - |\mathcal{N}_{\check{\mathbf{r}}_n^{(j)}}^{(j)}|} / M_n^{(j)}!$ . Here,  $\mathcal{N}_{\check{\mathbf{r}}_n^{(j)}}^{(j)}$  denotes the set of existing new PFs, i.e.,  $\mathcal{N}_{\check{\mathbf{r}}_n^{(j)}}^{(j)} \triangleq \{m \in \mathcal{M}_n^{(j)} : \check{r}_{m,n}^{(j)} = 1\}$ ;  $\mathcal{D}_{\mathbf{c}_n^{(j)}, \check{\mathbf{r}}_n^{(j)}}^{(j)}$  denotes the set of existing legacy PFs for PA  $j$ , i.e.,  $\mathcal{D}_{\mathbf{c}_n^{(j)}, \check{\mathbf{r}}_n^{(j)}}^{(j)} \triangleq \{k \in \mathcal{K}_{n-1}^{(j)} : \tilde{r}_{k,n}^{(j)} = 1, c_{k,n}^{(j)} \neq 0\}$ ; and  $\bar{\mathcal{D}}_{\mathbf{c}_n^{(j)}, \check{\mathbf{r}}_n^{(j)}}^{(j)} \triangleq \mathcal{K}_{n-1}^{(j)} \setminus \mathcal{D}_{\mathbf{c}_n^{(j)}, \check{\mathbf{r}}_n^{(j)}}^{(j)}$ . In addition, we define

$$\psi(\mathbf{c}_n^{(j)}) \triangleq \begin{cases} 0, & \exists k, k' \in \mathcal{K}_{n-1}^{(j)} \text{ with } k \neq k' \text{ such that } c_{k,n}^{(j)} = c_{k',n}^{(j)} \neq 0 \\ 1, & \text{otherwise,} \end{cases} \quad (9)$$

$$\Gamma_{\mathbf{c}_n^{(j)}}(\check{\mathbf{r}}_{m,n}^{(j)}) \triangleq \begin{cases} 0, & \check{r}_{m,n}^{(j)} = 1 \text{ and } \exists k \in \mathcal{K}_{n-1}^{(j)} \text{ such that } c_{k,n}^{(j)} = m \\ 1, & \text{otherwise.} \end{cases} \quad (10)$$

Finally,  $1(c)$  denotes the indicator function of the event  $c = 0$  (i.e.,  $1(c) = 1$  if  $c = 0$  and 0 otherwise). The functions  $\psi(\mathbf{c}_n^{(j)})$  and  $\Gamma_{\mathbf{c}_n^{(j)}}(\check{\mathbf{r}}_{m,n}^{(j)})$  enforce our DA assumption from Section III-B, i.e.,  $\psi(\mathbf{c}_n^{(j)})$  enforces  $p(\mathbf{c}_n^{(j)}, \check{\mathbf{r}}_n^{(j)}, M_n^{(j)} | \mathbf{x}_n, \tilde{\mathbf{y}}_n^{(j)}) = 0$  if any measurement is associated with more than one legacy PF, and  $\Gamma_{\mathbf{c}_n^{(j)}}(\check{\mathbf{r}}_{m,n}^{(j)})$  enforces  $p(\mathbf{c}_n^{(j)}, \check{\mathbf{r}}_n^{(j)}, M_n^{(j)} | \mathbf{x}_n, \tilde{\mathbf{y}}_n^{(j)}) = 0$  if a new PF is associated with a measurement  $m$  that is also associated with a legacy PF. At time  $n = 1$ , prior information on PAs and VAs can be incorporated by introducing legacy PFs. In the opposite case, there are no legacy PFs at  $n = 1$ , i.e.,  $\tilde{\mathbf{y}}_1^{(j)}$  is an empty vector, and thus  $p(\mathbf{c}_1^{(j)}, \check{\mathbf{r}}_1^{(j)}, M_1^{(j)} | \mathbf{x}_1, \tilde{\mathbf{y}}_1^{(j)}) = p(\mathbf{c}_1^{(j)}, \check{\mathbf{r}}_1^{(j)}, M_1^{(j)} | \mathbf{x}_1)$ . An expression of this pmf can be obtained by replacing in (8) (for  $n = 1$ ) all factors involving  $\tilde{\mathbf{y}}_1^{(j)}$  (or, equivalently,  $\tilde{\mathbf{a}}_1^{(j)}$  and  $\tilde{\mathbf{r}}_1^{(j)}$ ) by 1.

The states of newly detected features are assumed to be a priori independent and identically distributed (iid) according to some pdf  $f_{n,n}(\mathbf{a}_{\cdot,n}^{(j)} | \mathbf{x}_n)$ , whose calculation will be discussed in Section VI. (Here,  $\mathbf{a}_{\cdot,n}^{(j)} \in \mathbb{R}^2$  denotes a generic single-feature position.) The prior pdf of the states of new PFs for PA  $j$ ,  $\check{\mathbf{a}}_n^{(j)}$ , conditioned on  $\mathbf{x}_n$ ,  $\check{\mathbf{r}}_n^{(j)}$ , and  $M_n^{(j)}$  is then obtained as

$$f(\check{\mathbf{a}}_n^{(j)} | \mathbf{x}_n, \check{\mathbf{r}}_n^{(j)}, M_n^{(j)}) = \left( \prod_{m \in \mathcal{N}_{\check{\mathbf{r}}_n^{(j)}}^{(j)}} f_{n,n}(\check{\mathbf{a}}_{m,n}^{(j)} | \mathbf{x}_n) \right) \prod_{m' \in \bar{\mathcal{N}}_{\check{\mathbf{r}}_n^{(j)}}^{(j)}} f_D(\check{\mathbf{a}}_{m,n}^{(j)}), \quad (11)$$

where  $\bar{\mathcal{N}}_{\check{\mathbf{r}}_n^{(j)}}^{(j)} \triangleq \mathcal{M}_n^{(j)} \setminus \mathcal{N}_{\check{\mathbf{r}}_n^{(j)}}^{(j)}$ . Note that before the measurements are obtained,  $M_n^{(j)}$  and, thus, the length of the vectors  $\check{\mathbf{a}}_n^{(j)}$  and  $\check{\mathbf{r}}_n^{(j)}$  (which is  $M_n^{(j)}$ ) is random. In Section VI-B, a way to introduce prior information on new PFs (PAs and VAs) will be discussed.

We assume that for the agent state at time  $n = 1$ ,  $\mathbf{x}_1$ , an informative prior pdf  $f(\mathbf{x}_1)$  is available. We also assume that the new PF state vector  $\check{\mathbf{a}}_n^{(j)}$  and the DA vectors  $\mathbf{c}_n^{(j)}$  are conditionally independent given the legacy PF state vector  $\tilde{\mathbf{a}}_n^{(j)}$ . Let us next consider  $\mathbf{x}_{n'}$ ,  $\mathbf{y}_{n'}$ ,  $\mathbf{c}_{n'}$ , and the numbers-of-measurements vector  $\mathbf{m}_{n'} \triangleq [M_{n'}^{(1)} \cdots M_{n'}^{(J)}]^\top$  for all time steps  $n' = 1, \dots, n$ , and accordingly define the vector  $\mathbf{x}_{1:n} \triangleq [\mathbf{x}_1^\top \cdots \mathbf{x}_n^\top]^\top$  and similarly  $\mathbf{y}_{1:n}$ ,  $\mathbf{c}_{1:n}$ , and  $\mathbf{m}_{1:n}$ . We then obtain the joint prior pdf as

$$\begin{aligned} f(\mathbf{x}_{1:n}, \mathbf{y}_{1:n}, \mathbf{c}_{1:n}, \mathbf{m}_{1:n}) &= f(\mathbf{x}_1) \left( \prod_{j'=1}^J p(\mathbf{c}_1^{(j')}, \check{\mathbf{r}}_1^{(j')}, M_1^{(j')} | \mathbf{x}_1, \tilde{\mathbf{y}}_1^{(j')}) \right) \prod_{n'=2}^n f(\mathbf{x}_{n'} | \mathbf{x}_{n'-1}) \\ &\quad \times \prod_{j=1}^J f(\tilde{\mathbf{y}}_{n'}^{(j)} | \mathbf{y}_{n'-1}^{(j)}) f(\check{\mathbf{a}}_{n'}^{(j)} | \mathbf{x}_{n'}, \check{\mathbf{r}}_{n'}^{(j)}, M_{n'}^{(j)}) p(\mathbf{c}_{n'}^{(j)}, \check{\mathbf{r}}_{n'}^{(j)}, M_{n'}^{(j)} | \mathbf{x}_{n'}, \tilde{\mathbf{y}}_{n'}^{(j)}), \end{aligned} \quad (12)$$

where the last three factors are given by (6) and (7); (11); and (8), respectively.

### E. Likelihood Function

The statistical dependency of the measurements (MPC parameter estimates)  $\mathbf{z}_{m,n}^{(j)}$  on the states  $\mathbf{x}_n$  and  $\mathbf{a}_{k,n}^{(j)}$  is characterized by the conditional pdf  $f(\mathbf{z}_{m,n}^{(j)}|\mathbf{x}_n, \mathbf{a}_{k,n}^{(j)})$ . This pdf depends on the concrete measurement model; an example will be considered in Section VII. The pdf  $f(\mathbf{z}_{m,n}^{(j)}|\mathbf{x}_n, \mathbf{a}_{k,n}^{(j)})$  is a central element in the conditional pdf of the total measurement vector  $\mathbf{z}_n \triangleq [\mathbf{z}_n^{(1)\top} \dots \mathbf{z}_n^{(J)\top}]^\top$  given  $\mathbf{x}_n, \tilde{\mathbf{y}}_n, \check{\mathbf{y}}_n, \mathbf{c}_n$ , and  $\mathbf{m}_n$ . Assuming that the  $\mathbf{z}_n^{(j)}$  are conditionally independent across  $j$  given  $\mathbf{x}_n, \tilde{\mathbf{y}}_n, \check{\mathbf{y}}_n, \mathbf{c}_n$ , and  $\mathbf{m}_n$  [29], we obtain

$$f(\mathbf{z}_n|\mathbf{x}_n, \tilde{\mathbf{y}}_n, \check{\mathbf{y}}_n, \mathbf{c}_n, \mathbf{m}_n) = \prod_{j=1}^J f(\mathbf{z}_n^{(j)}|\mathbf{x}_n, \tilde{\mathbf{y}}_n^{(j)}, \check{\mathbf{y}}_n^{(j)}, \mathbf{c}_n^{(j)}, M_n^{(j)}), \quad (13)$$

where [29]

$$\begin{aligned} f(\mathbf{z}_n^{(j)}|\mathbf{x}_n, \tilde{\mathbf{y}}_n^{(j)}, \check{\mathbf{y}}_n^{(j)}, \mathbf{c}_n^{(j)}, M_n^{(j)}) &= \left( \prod_{m=1}^{M_n^{(j)}} f_{\text{FA}}(\mathbf{z}_{m,n}^{(j)}) \right) \left( \prod_{k \in \mathcal{D}_{\mathbf{c}_n^{(j)}, \tilde{\mathbf{r}}_n^{(j)}}} \frac{f(\mathbf{z}_{c_{k,n}^{(j)}, n}^{(j)}|\mathbf{x}_n, \tilde{\mathbf{a}}_{k,n}^{(j)})}{f_{\text{FA}}(\mathbf{z}_{c_{k,n}^{(j)}, n}^{(j)})} \right) \\ &\times \prod_{m' \in \mathcal{N}_{\tilde{\mathbf{r}}_n^{(j)}}} \frac{f(\mathbf{z}_{m',n}^{(j)}|\mathbf{x}_n, \check{\mathbf{a}}_{m',n}^{(j)})}{f_{\text{FA}}(\mathbf{z}_{m',n}^{(j)})}. \end{aligned} \quad (14)$$

In particular, at  $n = 1$ ,  $f(\mathbf{z}_1^{(j)}|\mathbf{x}_1, \tilde{\mathbf{y}}_1^{(j)}, \check{\mathbf{y}}_1^{(j)}, \mathbf{c}_1^{(j)}, M_1^{(j)}) = f(\mathbf{z}_1^{(j)}|\mathbf{x}_1, \check{\mathbf{y}}_1^{(j)}, \mathbf{c}_1^{(j)}, M_1^{(j)})$ . An expression of this pdf can be obtained by replacing in (14) (for  $n = 1$ ) all factors involving  $\tilde{\mathbf{y}}_1^{(j)}$  (or, equivalently,  $\tilde{\mathbf{a}}_1^{(j)}$  and  $\tilde{\mathbf{r}}_1^{(j)}$ ) by 1.

Let us consider  $f(\mathbf{z}_n^{(j)}|\mathbf{x}_n, \tilde{\mathbf{y}}_n^{(j)}, \check{\mathbf{y}}_n^{(j)}, \mathbf{c}_n^{(j)}, M_n^{(j)})$  as a *likelihood function*, i.e., a function of  $\mathbf{x}_n, \tilde{\mathbf{y}}_n^{(j)}, \check{\mathbf{y}}_n^{(j)}, \mathbf{c}_n^{(j)}$ , and  $M_n^{(j)}$ , for observed  $\mathbf{z}_n^{(j)}$ . If  $\mathbf{z}_n^{(j)}$  is observed and therefore fixed, also  $M_n^{(j)}$  is fixed, and we can rewrite (14), up to a constant normalization factor, as

$$f(\mathbf{z}_n^{(j)}|\mathbf{x}_n, \tilde{\mathbf{y}}_n^{(j)}, \check{\mathbf{y}}_n^{(j)}, \mathbf{c}_n^{(j)}, M_n^{(j)}) \propto \left( \prod_{k=1}^{K_n^{(j)}} g_1(\mathbf{x}_n, \tilde{\mathbf{a}}_{k,n}^{(j)}, \tilde{\mathbf{r}}_{k,n}^{(j)}, \mathbf{c}_{k,n}^{(j)}; \mathbf{z}_n^{(j)}) \right) \prod_{m \in \mathcal{N}_{\tilde{\mathbf{r}}_n^{(j)}}} \frac{f(\mathbf{z}_{m,n}^{(j)}|\mathbf{x}_n, \check{\mathbf{a}}_{m,n}^{(j)})}{f_{\text{FA}}(\mathbf{z}_{m,n}^{(j)})}. \quad (15)$$

Here, the factors  $g_1(\mathbf{x}_n, \tilde{\mathbf{a}}_{k,n}^{(j)}, \tilde{\mathbf{r}}_{k,n}^{(j)}, \mathbf{c}_{k,n}^{(j)}; \mathbf{z}_n^{(j)})$  are defined as

$$g_1(\mathbf{x}_n, \tilde{\mathbf{a}}_{k,n}^{(j)}, \tilde{\mathbf{r}}_{k,n}^{(j)}, \mathbf{c}_{k,n}^{(j)}; \mathbf{z}_n^{(j)}) \triangleq \begin{cases} \frac{f(\mathbf{z}_{m,n}^{(j)}|\mathbf{x}_n, \tilde{\mathbf{a}}_{k,n}^{(j)})}{f_{\text{FA}}(\mathbf{z}_{m,n}^{(j)})}, & \mathbf{c}_{k,n}^{(j)} \in \mathcal{M}_n^{(j)} \\ 1, & \mathbf{c}_{k,n}^{(j)} = 0 \end{cases} \quad (16)$$

$$g_1(\mathbf{x}_n, \tilde{\mathbf{a}}_{k,n}^{(j)}, 0, \mathbf{c}_{k,n}^{(j)}; \mathbf{z}_n^{(j)}) \triangleq 1.$$

Finally, the likelihood function for  $\mathbf{z}_{1:n} \triangleq [\mathbf{z}_1^T \cdots \mathbf{z}_n^T]^T$ , involving the measurements  $\mathbf{z}_{m,n'}^{(j)}$  of all PAs  $j = 1, \dots, J$  and all time steps  $n' = 1, \dots, n$ , can be derived similarly to (12); one obtains

$$f(\mathbf{z}_{1:n} | \mathbf{x}_{1:n}, \mathbf{y}_{1:n}, \mathbf{c}_{1:n}, \mathbf{m}_{1:n}) \propto \prod_{j=1}^J \left( \prod_{m \in \mathcal{N}_{\tilde{\mathbf{r}}_1}^{(j)}} \frac{f(\mathbf{z}_{m,1}^{(j)} | \mathbf{x}_1, \check{\mathbf{a}}_{m,1}^{(j)})}{f_{\text{FA}}(\mathbf{z}_{m,1}^{(j)})} \right) \prod_{n'=2}^n \left( \prod_{m' \in \mathcal{N}_{\tilde{\mathbf{r}}_{n'}}^{(j)}} \frac{f(\mathbf{z}_{m',n'}^{(j)} | \mathbf{x}_{n'}, \check{\mathbf{a}}_{m',n'}^{(j)})}{f_{\text{FA}}(\mathbf{z}_{m',n'}^{(j)})} \right) \\ \times \prod_{k=1}^{K_{n'}^{(j)}} g_1(\mathbf{x}_{n'}, \check{\mathbf{a}}_{k,n'}^{(j)}, \check{r}_{k,n'}^{(j)}, c_{k,n'}^{(j)}; \mathbf{z}_{n'}^{(j)}). \quad (17)$$

#### IV. JOINT POSTERIOR PDF AND FACTOR GRAPH

##### A. Redundant Formulation of the Exclusion Constraint

The proposed BP algorithm is based on a redundant formulation of probabilistic DA that involves both the feature-oriented DA vectors  $\mathbf{c}_n^{(j)}$  and the measurement-oriented DA vectors  $\mathbf{b}_n^{(j)}$  [36], [38]. To obtain a corresponding probabilistic description and, in turn, a factor graph, we formally replace the exclusion constraint factor  $\psi(\mathbf{c}_n^{(j)})$  involved in the prior pmf in (8) by

$$\psi(\mathbf{c}_n^{(j)}, \mathbf{b}_n^{(j)}) \triangleq \prod_{k=1}^{K_n^{(j)}} \prod_{m=1}^{M_n^{(j)}} \psi(c_{k,n}^{(j)}, b_{m,n}^{(j)}), \quad (18)$$

with the indicator function

$$\psi(c_{k,n}^{(j)}, b_{m,n}^{(j)}) \triangleq \begin{cases} 0, & c_{k,n}^{(j)} = m, b_{m,n}^{(j)} \neq k \text{ or } b_{m,n}^{(j)} = k, c_{k,n}^{(j)} \neq m \\ 1, & \text{else.} \end{cases} \quad (19)$$

The resulting modified prior pmf  $p(\mathbf{c}_n^{(j)}, \mathbf{b}_n^{(j)}, \check{\mathbf{r}}_n^{(j)}, M_n^{(j)} | \mathbf{x}_n, \tilde{\mathbf{y}}_n^{(j)})$  is related to the original prior pmf  $p(\mathbf{c}_n^{(j)}, \check{\mathbf{r}}_n^{(j)}, M_n^{(j)} | \mathbf{x}_n, \tilde{\mathbf{y}}_n^{(j)})$  in (8) according to  $p(\mathbf{c}_n^{(j)}, \check{\mathbf{r}}_n^{(j)}, M_n^{(j)} | \mathbf{x}_n, \tilde{\mathbf{y}}_n^{(j)}) = \sum_{\mathbf{b}_n^{(j)}} p(\mathbf{c}_n^{(j)}, \mathbf{b}_n^{(j)}, \check{\mathbf{r}}_n^{(j)}, M_n^{(j)} | \mathbf{x}_n, \tilde{\mathbf{y}}_n^{(j)})$ , where the summation is over all  $\mathbf{b}_n^{(j)} \in \{0, 1, \dots, K_n^{(j)}\}^{M_n^{(j)}}$ .

Let us now consider the product of the likelihood function  $f(\mathbf{z}_n^{(j)} | \mathbf{x}_n, \tilde{\mathbf{y}}_n^{(j)}, \check{\mathbf{y}}_n^{(j)}, \mathbf{c}_n^{(j)}, M_n^{(j)})$  in (15), the prior pdf of the new PF states  $f(\check{\mathbf{a}}_n^{(j)} | \mathbf{x}_n, \check{\mathbf{r}}_n^{(j)}, M_n^{(j)})$  in (11), and the modified prior pmf  $p(\mathbf{c}_n^{(j)}, \mathbf{b}_n^{(j)}, \check{\mathbf{r}}_n^{(j)}, M_n^{(j)} | \mathbf{x}_n, \tilde{\mathbf{y}}_n^{(j)})$ . We obtain

$$f(\mathbf{z}_n^{(j)} | \mathbf{x}_n, \tilde{\mathbf{y}}_n^{(j)}, \check{\mathbf{y}}_n^{(j)}, \mathbf{c}_n^{(j)}, M_n^{(j)}) f(\check{\mathbf{a}}_n^{(j)} | \mathbf{x}_n, \check{\mathbf{r}}_n^{(j)}, M_n^{(j)}) p(\mathbf{c}_n^{(j)}, \mathbf{b}_n^{(j)}, \check{\mathbf{r}}_n^{(j)}, M_n^{(j)} | \mathbf{x}_n, \tilde{\mathbf{y}}_n^{(j)}) \\ \propto \psi(\mathbf{c}_n^{(j)}, \mathbf{b}_n^{(j)}) \left( \prod_{k=1}^{K_n^{(j)}} g(\mathbf{x}_n, \check{\mathbf{a}}_{k,n}^{(j)}, \check{r}_{k,n}^{(j)}, c_{k,n}^{(j)}; \mathbf{z}_n^{(j)}) \right) \left( \prod_{m' \in \mathcal{N}_{\tilde{\mathbf{r}}_n}^{(j)}} f_{\text{D}}(\check{\mathbf{a}}_{m',n}^{(j)}) \right) \\ \times \prod_{m \in \mathcal{N}_{\tilde{\mathbf{r}}_n}^{(j)}} \frac{\mu_{n,n}^{(j)} f_{n,n}(\check{\mathbf{a}}_{m,n}^{(j)} | \mathbf{x}_n) \Gamma_{\mathbf{c}_n^{(j)}}(\check{r}_{m,n}^{(j)}) f(\mathbf{z}_{m,n}^{(j)} | \mathbf{x}_n, \check{\mathbf{a}}_{m,n}^{(j)})}{f_{\text{FA}}(\mathbf{z}_{m,n}^{(j)})}. \quad (20)$$

Here,  $g(\mathbf{x}_n, \tilde{\mathbf{a}}_{k,n}^{(j)}, \tilde{r}_{k,n}^{(j)}, c_{k,n}^{(j)}; \mathbf{z}_n^{(j)}) \triangleq g_1(\mathbf{x}_n, \tilde{\mathbf{a}}_{k,n}^{(j)}, \tilde{r}_{k,n}^{(j)}, c_{k,n}^{(j)}; \mathbf{z}_n^{(j)}) g_2(\mathbf{x}_n, \tilde{\mathbf{a}}_{k,n}^{(j)}, \tilde{r}_{k,n}^{(j)}, c_{k,n}^{(j)}; M_n^{(j)})$ , where  $g_1(\mathbf{x}_n, \tilde{\mathbf{a}}_{k,n}^{(j)}, \tilde{r}_{k,n}^{(j)}, c_{k,n}^{(j)}; \mathbf{z}_n^{(j)})$  was defined in (16) and  $g_2(\mathbf{x}_n, \tilde{\mathbf{a}}_{k,n}^{(j)}, \tilde{r}_{k,n}^{(j)}, c_{k,n}^{(j)}; M_n^{(j)})$  is defined as

$$g_2(\mathbf{x}_n, \tilde{\mathbf{a}}_{k,n}^{(j)}, 1, c_{k,n}^{(j)}; M_n^{(j)}) \triangleq \begin{cases} \frac{P_d^{(j)}(\mathbf{x}_n, \tilde{\mathbf{a}}_{k,n}^{(j)})}{\mu_{\text{FA}}^{(j)}}, & c_{k,n}^{(j)} \in \mathcal{M}_n^{(j)} \\ 1 - P_d^{(j)}(\mathbf{x}_n, \tilde{\mathbf{a}}_{k,n}^{(j)}), & c_{k,n}^{(j)} = 0 \end{cases} \quad (21)$$

$$g_2(\mathbf{x}_n, \tilde{\mathbf{a}}_{k,n}^{(j)}, 0, c_{k,n}^{(j)}; M_n^{(j)}) \triangleq 1(c_{k,n}^{(j)}).$$

One thus obtains for  $g(\mathbf{x}_n, \tilde{\mathbf{a}}_{k,n}^{(j)}, \tilde{r}_{k,n}^{(j)}, c_{k,n}^{(j)}; \mathbf{z}_n^{(j)})$

$$g(\mathbf{x}_n, \tilde{\mathbf{a}}_{k,n}^{(j)}, 1, c_{k,n}^{(j)}; \mathbf{z}_n^{(j)}) = \begin{cases} \frac{P_d^{(j)}(\mathbf{x}_n, \tilde{\mathbf{a}}_{k,n}^{(j)}) f(\mathbf{z}_{m,n}^{(j)} | \mathbf{x}_n, \tilde{\mathbf{a}}_{k,n}^{(j)})}{\mu_{\text{FA}}^{(j)} f_{\text{FA}}(\mathbf{z}_{m,n}^{(j)})}, & c_{k,n}^{(j)} \in \mathcal{M}_n^{(j)} \\ 1 - P_d^{(j)}(\mathbf{x}_n, \tilde{\mathbf{a}}_{k,n}^{(j)}), & c_{k,n}^{(j)} = 0 \end{cases} \quad (22)$$

$$g(\mathbf{x}_n, \tilde{\mathbf{a}}_{k,n}^{(j)}, 0, c_{k,n}^{(j)}; \mathbf{z}_n^{(j)}) = 1(c_{k,n}^{(j)}).$$

For a choice of  $\mathbf{c}_n^{(j)}$  and  $\mathbf{b}_n^{(j)}$  that is valid in the sense that  $p(\mathbf{c}_n^{(j)}, \mathbf{b}_n^{(j)}, \check{\mathbf{r}}_n^{(j)}, M_n^{(j)} | \mathbf{x}_n, \check{\mathbf{y}}_n^{(j)}) \neq 0$ , the exclusion constraint expressed by  $\Gamma_{\mathbf{c}_n^{(j)}}(\check{r}_{m,n}^{(j)})$  is satisfied, i.e.,  $\Gamma_{\mathbf{c}_n^{(j)}}(\check{r}_{m,n}^{(j)}) = 1$ , if and only if both  $b_{m,n}^{(j)} = 0$  and  $\check{r}_{m,n}^{(j)} = 1$ . Therefore, in (20), we can summarize the products over all  $m \in \mathcal{N}_{\check{\mathbf{r}}_n^{(j)}}^{(j)}$  and over all  $m' \in \bar{\mathcal{N}}_{\check{\mathbf{r}}_n^{(j)}}^{(j)}$  by a product over all  $m \in \mathcal{M}_n^{(j)} = \{1, \dots, M_n^{(j)}\}$ . More specifically, we can rewrite (20) as

$$\begin{aligned} & f(\mathbf{z}_n^{(j)} | \mathbf{x}_n, \check{\mathbf{y}}_n^{(j)}, \check{\mathbf{y}}_n^{(j)}, \mathbf{c}_n^{(j)}, M_n^{(j)}) f(\check{\mathbf{a}}_n^{(j)} | \mathbf{x}_n, \check{\mathbf{r}}_n^{(j)}, M_n^{(j)}) p(\mathbf{c}_n^{(j)}, \mathbf{b}_n^{(j)}, \check{\mathbf{r}}_n^{(j)}, M_n^{(j)} | \mathbf{x}_n, \check{\mathbf{y}}_n^{(j)}) \\ & \propto \psi(\mathbf{c}_n^{(j)}, \mathbf{b}_n^{(j)}) \left( \prod_{k=1}^{K_n^{(j)}} g(\mathbf{x}_n, \tilde{\mathbf{a}}_{k,n}^{(j)}, \tilde{r}_{k,n}^{(j)}, c_{k,n}^{(j)}; \mathbf{z}_n^{(j)}) \right) \prod_{m=1}^{M_n^{(j)}} h(\mathbf{x}_n, \check{\mathbf{a}}_{m,n}^{(j)}, \check{r}_{m,n}^{(j)}, b_{m,n}^{(j)}; \mathbf{z}_n^{(j)}), \quad (23) \end{aligned}$$

where  $h(\mathbf{x}_n, \check{\mathbf{a}}_{m,n}^{(j)}, \check{r}_{m,n}^{(j)}, b_{m,n}^{(j)}; \mathbf{z}_n^{(j)})$  is defined as

$$h(\mathbf{x}_n, \check{\mathbf{a}}_{m,n}^{(j)}, 1, b_{m,n}^{(j)}; \mathbf{z}_n^{(j)}) \triangleq \begin{cases} 0, & b_{m,n}^{(j)} \in \mathcal{K}_n^{(j)} \\ \frac{\mu_{n,n}^{(j)} f_{n,n}(\check{\mathbf{a}}_{m,n}^{(j)} | \mathbf{x}_n) f(\mathbf{z}_{m,n}^{(j)} | \mathbf{x}_n, \check{\mathbf{a}}_{m,n}^{(j)})}{\mu_{\text{FA}}^{(j)} f_{\text{FA}}(\mathbf{z}_{m,n}^{(j)})}, & b_{m,n}^{(j)} = 0 \end{cases} \quad (24)$$

$$h(\mathbf{x}_n, \check{\mathbf{a}}_{m,n}^{(j)}, 0, b_{m,n}^{(j)}; \mathbf{z}_n^{(j)}) \triangleq f_D(\check{\mathbf{a}}_{m,n}^{(j)}).$$

The calculation of  $\mu_{n,n}^{(j)} f_{n,n}(\check{\mathbf{a}}_{m,n}^{(j)} | \mathbf{x}_n)$  will be discussed in Section VI.

## B. Joint Posterior pdf

Using Bayes' rule and independence assumptions related to the state-transition pdfs (see Section III-C), the prior pdfs (see Section III-D), and the likelihood model (see Section III-E), the joint posterior pdf of  $\mathbf{x}_{n'}$ ,  $\tilde{\mathbf{y}}_{n'}$ ,  $\check{\mathbf{y}}_{n'}$ ,  $\mathbf{c}_{n'}$ , and  $\mathbf{b}_{n'}$  for all  $n' = 1, \dots, n$  is obtained as

$$\begin{aligned}
& f(\mathbf{x}_{1:n}, \mathbf{y}_{1:n}, \mathbf{c}_{1:n}, \mathbf{b}_{1:n}, \mathbf{m}_{1:n} | \mathbf{z}_{1:n}) \\
& \propto f(\mathbf{z}_{1:n} | \mathbf{x}_{1:n}, \mathbf{y}_{1:n}, \mathbf{c}_{1:n}, \mathbf{m}_{1:n}) f(\mathbf{x}_{1:n}, \mathbf{y}_{1:n}, \mathbf{c}_{1:n}, \mathbf{m}_{1:n}) \\
& = f(\mathbf{x}_1) \left( \prod_{j'=1}^J f(\mathbf{z}_1^{(j')} | \mathbf{x}_1, \check{\mathbf{y}}_1^{(j')}, \mathbf{c}_1^{(j')}, M_1^{(j')}) f(\check{\mathbf{y}}_1^{(j')}, \mathbf{c}_1^{(j')}, M_1^{(j')}) \right) \prod_{n'=2}^n f(\mathbf{x}_{n'} | \mathbf{x}_{n'-1}) \prod_{j=1}^J f(\tilde{\mathbf{y}}_{n'}^{(j)} | \mathbf{y}_{n'-1}^{(j)}) \\
& \quad \times f(\mathbf{z}_{n'}^{(j)} | \mathbf{x}_{n'}, \tilde{\mathbf{y}}_{n'}^{(j)}, \check{\mathbf{y}}_{n'}^{(j)}, \mathbf{c}_{n'}^{(j)}, M_{n'}^{(j)}) f(\check{\mathbf{a}}_{n'}^{(j)} | \mathbf{x}_{n'}, \check{\mathbf{r}}_{n'}^{(j)}, M_{n'}^{(j)}) p(\mathbf{c}_{n'}^{(j)}, \mathbf{b}_{n'}^{(j)}, \check{\mathbf{r}}_{n'}^{(j)}, M_{n'}^{(j)} | \mathbf{x}_{n'}, \tilde{\mathbf{y}}_{n'}^{(j)}). \quad (25)
\end{aligned}$$

Inserting expression (23) yields

$$\begin{aligned}
& f(\mathbf{x}_{1:n}, \mathbf{y}_{1:n}, \mathbf{c}_{1:n}, \mathbf{b}_{1:n}, \mathbf{m}_{1:n} | \mathbf{z}_{1:n}) \\
& \propto f(\mathbf{x}_1) \left( \prod_{j'=1}^J \prod_{m'=1}^{M_1^{(j')}} h(\mathbf{x}_1, \check{\mathbf{a}}_{m',1}^{(j')}, \check{\mathbf{r}}_{m',1}^{(j')}, b_{m',1}^{(j')}; \mathbf{z}_1^{(j')}) \right) \prod_{n'=2}^n f(\mathbf{x}_{n'} | \mathbf{x}_{n'-1}) \prod_{j=1}^J \psi(\mathbf{c}_{n'}^{(j)}, \mathbf{b}_{n'}^{(j)}) \\
& \quad \times \left( \prod_{m=1}^{M_{n'}^{(j)}} h(\mathbf{x}_{n'}, \check{\mathbf{a}}_{m,n'}^{(j)}, \check{\mathbf{r}}_{m,n'}^{(j)}, b_{m,n'}^{(j)}; \mathbf{z}_{n'}^{(j)}) \right) \prod_{k=1}^{K_{n'-1}^{(j)}} f(\tilde{\mathbf{y}}_{k,n'}^{(j)} | \mathbf{y}_{k,n'-1}^{(j)}) g(\mathbf{x}_{n'}, \tilde{\mathbf{a}}_{k,n'}^{(j)}, \tilde{\mathbf{r}}_{k,n'}^{(j)}, c_{k,n'}^{(j)}; \mathbf{z}_{n'}^{(j)}). \quad (26)
\end{aligned}$$

This factorization of the joint posterior pdf is represented by the factor graph [34], [35] shown in Fig. 2.

## V. BP ALGORITHM FOR SLAM

In this section, we first discuss the procedure used for PF detection and state estimation. Subsequently, we develop a BP message passing algorithm for approximate calculation of the marginal posterior distributions required for detection and estimation.

### A. Detection and Estimation

Our goal is to estimate the agent state  $\mathbf{x}_n$  and to detect and estimate the PF states  $\mathbf{a}_{k,n}^{(j)}$  from all the past and present measurements, i.e., from the total measurement vector  $\mathbf{z}_{1:n}$ . In the Bayesian framework, estimation of  $\mathbf{x}_n$  at time  $n$  is based on the posterior pdf  $f(\mathbf{x}_n | \mathbf{z}_{1:n})$ . More specifically, we will develop an approximate calculation of the minimum mean-square error (MMSE) estimator [48]

$$\hat{\mathbf{x}}_n^{\text{MMSE}} \triangleq \int \mathbf{x}_n f(\mathbf{x}_n | \mathbf{z}_{1:n}) d\mathbf{x}_n. \quad (27)$$

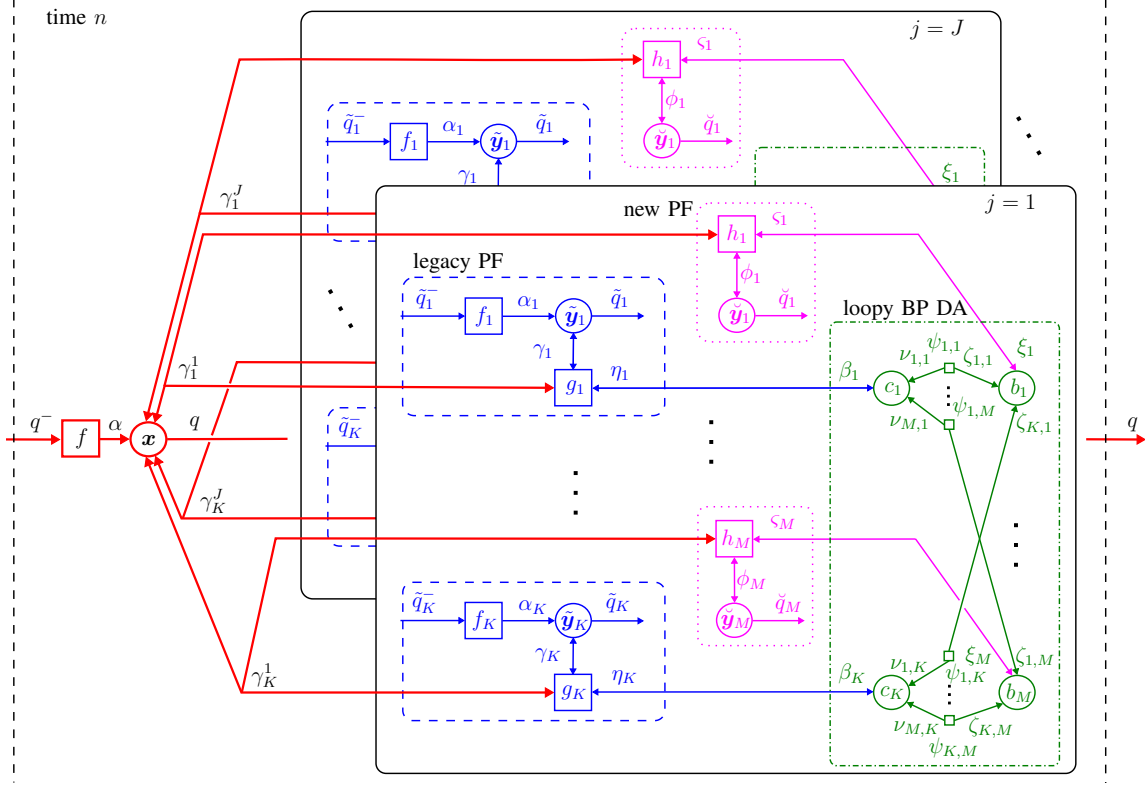


Fig. 2: Factor graph representing the factorization of the joint posterior pdf in (26). All the factor nodes, variable nodes, and messages related to the agent state are represented in red boldface style, those related to the legacy PF states are represented by the blue parts contained in dashed boxes, those related to the new PF states are represented by the magenta parts contained in dotted boxes, and those related to loopy BP DA are represented by the green parts contained in dashed-dotted boxes. The following short notations are used:  $K \triangleq K_n^{(j)}$ ,  $M \triangleq M_n^{(j)}$ ,  $\mathbf{x} \triangleq \mathbf{x}_n$ ,  $\tilde{\mathbf{y}}_k \triangleq \tilde{\mathbf{y}}_{k,n}^{(j)}$ ,  $\check{\mathbf{y}}_m \triangleq \check{\mathbf{y}}_{m,n}^{(j)}$ ,  $b_m \triangleq b_{m,n}^{(j)}$ ,  $c_k \triangleq c_{k,n}^{(j)}$ ,  $\psi_{k,m} \triangleq \psi(c_{k,n}^{(j)}, b_{m,n}^{(j)})$ ,  $g_k \triangleq g(\mathbf{x}_n, \tilde{\mathbf{a}}_{k,n}^{(j)}, \tilde{r}_{k,n}^{(j)}, c_{k,n}^{(j)}; \mathbf{z}_n^{(j)})$ ,  $h_m \triangleq h(\mathbf{x}_n, \check{\mathbf{a}}_{m,n}^{(j)}, \check{r}_{m,n}^{(j)}, b_{m,n}^{(j)}; \mathbf{z}_n^{(j)})$ ,  $f \triangleq f(\mathbf{x}_n | \mathbf{x}_{n-1})$ ,  $f_k \triangleq f(\tilde{\mathbf{y}}_{k,n}^{(j)} | \mathbf{y}_{k,n-1}^{(j)})$ ,  $\alpha \triangleq \alpha(\mathbf{x}_n)$ ,  $\alpha_k \triangleq \alpha_k(\tilde{\mathbf{a}}_{k,n}^{(j)}, \tilde{r}_{k,n}^{(j)})$ ,  $q^- \triangleq q(\mathbf{x}_{n-1})$ ,  $q \triangleq q(\mathbf{x}_n)$ ,  $\tilde{q}_k^- \triangleq \tilde{q}(\tilde{\mathbf{a}}_{k,n-1}^{(j)}, \tilde{r}_{k,n-1}^{(j)})$ ,  $\tilde{q}_k \triangleq \tilde{q}(\tilde{\mathbf{a}}_{k,n}^{(j)}, \tilde{r}_{k,n}^{(j)})$ ,  $\check{q}_m \triangleq \check{q}(\check{\mathbf{a}}_{m,n}^{(j)}, \check{r}_{m,n}^{(j)})$ ,  $\beta_k \triangleq \beta(c_{k,n}^{(j)})$ ,  $\xi_m \triangleq \xi(b_{m,n}^{(j)})$ ,  $\eta_k \triangleq \eta(c_{k,n}^{(j)})$ ,  $\varsigma_m \triangleq \varsigma(b_{m,n}^{(j)})$ ,  $\nu_{m,k} \triangleq \nu_{m \rightarrow k}^{(p)}(c_{k,n}^{(j)})$ ,  $\zeta_{k,m} \triangleq \zeta_{k \rightarrow m}^{(p)}(b_{m,n}^{(j)})$ ,  $\gamma_k^j \triangleq \gamma_k^{(j)}(\mathbf{x}_n)$ ,  $\gamma_k \triangleq \gamma(\tilde{\mathbf{a}}_{k,n}^{(j)}, \tilde{r}_{k,n}^{(j)})$ , and  $\phi_m \triangleq \phi(\check{\mathbf{a}}_{m,n}^{(j)}, \check{r}_{m,n}^{(j)})$ .

Furthermore, detecting (i.e., determining the existence of) PF  $k \in \mathcal{K}_n^{(j)}$  at time  $n$  is based on the posterior existence probability  $p(r_{k,n}^{(j)} = 1 | \mathbf{z}_{1:n})$ . This probability can be obtained from the posterior pdf of the augmented PF state,  $f(\mathbf{y}_{k,n}^{(j)} | \mathbf{z}_{1:n}) = f(\mathbf{a}_{k,n}^{(j)}, r_{k,n}^{(j)} | \mathbf{z}_{1:n})$ , by a marginalization

$$p(r_{k,n}^{(j)} = 1 | \mathbf{z}_{1:n}) = \int f(\mathbf{a}_{k,n}^{(j)}, r_{k,n}^{(j)} = 1 | \mathbf{z}_{1:n}) d\mathbf{a}_{k,n}^{(j)}. \quad (28)$$

Then PF  $k$  is defined to be detected at time  $n$  if  $p(r_{k,n}^{(j)} = 1 | \mathbf{z}_{1:n}) > P_{\text{det}}$ , where  $P_{\text{det}}$  is a detection threshold. The states  $\mathbf{a}_{k,n}^{(j)}$  of the detected PFs are estimated as

$$\hat{\mathbf{a}}_{k,n}^{(j)\text{MMSE}} \triangleq \int \mathbf{a}_{k,n}^{(j)} f(\mathbf{a}_{k,n}^{(j)} | r_{k,n}^{(j)} = 1, \mathbf{z}_{1:n}) d\mathbf{a}_{k,n}^{(j)}, \quad (29)$$

where

$$f(\mathbf{a}_{k,n}^{(j)} | r_{k,n}^{(j)} = 1, \mathbf{z}_{1:n}) = \frac{f(\mathbf{a}_{k,n}^{(j)}, r_{k,n}^{(j)} = 1 | \mathbf{z}_{1:n})}{p(r_{k,n}^{(j)} = 1 | \mathbf{z}_{1:n})}. \quad (30)$$

The posterior existence probabilities  $p(r_{k,n}^{(j)} = 1 | \mathbf{z}_{1:n})$  in (28) are also used in a different context. To prevent an indefinite increase of the total number of PFs for PA  $j$  due to (2), i.e.,  $K_n^{(j)} = K_{n-1}^{(j)} + M_n^{(j)}$ , a pruning of the PFs is employed. More specifically, PF  $k$  is retained only if  $p(r_{k,n}^{(j)} = 1 | \mathbf{z}_{1:n})$  exceeds a suitably chosen pruning threshold  $P_{\text{prun}}$ .

### B. BP Message Passing Algorithm

The expressions (27), (28), and (29) involve the posterior pdfs  $f(\mathbf{x}_n | \mathbf{z}_{1:n})$  and  $f(\mathbf{a}_{k,n}^{(j)}, r_{k,n}^{(j)} | \mathbf{z}_{1:n})$ , which are marginal pdfs of the joint posterior pdf  $f(\mathbf{x}_{1:n}, \mathbf{y}_{1:n}, \mathbf{c}_{1:n}, \mathbf{b}_{1:n}, \mathbf{m}_{1:n} | \mathbf{z}_{1:n})$  in (26). However, direct marginalization of the joint posterior pdf is infeasible. Therefore, the marginal pdfs  $f(\mathbf{x}_n | \mathbf{z}_{1:n})$  and  $f(\mathbf{a}_{k,n}^{(j)}, r_{k,n}^{(j)} | \mathbf{z}_{1:n})$  are approximated by means of an efficient BP message passing algorithm. This algorithm is derived by applying the sum-product algorithm [35] to the factor graph in Fig. 2. Since the factor graph contains loops, the sum-product algorithm is used in an iterative manner, and the resulting beliefs are only approximations of the respective posterior pdfs. Furthermore, there is no canonical order in which the messages should be computed, and different orders may lead to different beliefs [35]. In our method, we choose the order according to the following rules: (i) Messages are not passed backward in time; (ii) *iterative* message passing is only performed for DA, and only for each time step and for each PA separately (i.e., in particular, for the loops connecting different PAs, we only perform a single message passing iteration); (iii) along an edge connecting an agent state variable node and a new PF state variable node, messages are only sent from the former to the latter. Using the message passing schedule resulting from these rules, the sum-product algorithm leads to the message passing and calculation scheme presented in what follows; see also Fig. 2. In this scheme, similarly to the “dummy pdfs” introduced in Section III-A, we consider BP messages  $\phi(\mathbf{y}_{k,n}^{(j)}) = \phi(\mathbf{a}_{k,n}^{(j)}, r_{k,n}^{(j)})$  also for the non-existing PF states, i.e., for  $r_{k,n}^{(j)} = 0$ . We define these messages by setting  $\phi(\mathbf{a}_{k,n}^{(j)}, 0) = \phi_{k,n}^{(j)}$  (note that these BP messages are not pdfs and thus are not required to integrate to 1).

First, a prediction step is performed. The prediction message for the agent state is obtained as

$$\alpha(\mathbf{x}_n) = \int f(\mathbf{x}_n | \mathbf{x}_{n-1}) q(\mathbf{x}_{n-1}) d\mathbf{x}_{n-1}, \quad (31)$$

and the prediction message for the legacy PFs is obtained as

$$\alpha_k(\tilde{\mathbf{a}}_{k,n}^{(j)}, \tilde{r}_{k,n}^{(j)}) = \sum_{r_{k,n-1}^{(j)} \in \{0,1\}} \int f(\tilde{\mathbf{a}}_{k,n}^{(j)}, \tilde{r}_{k,n}^{(j)} | \mathbf{a}_{k,n-1}^{(j)}, r_{k,n-1}^{(j)}) \tilde{q}(\mathbf{a}_{k,n-1}^{(j)}, r_{k,n-1}^{(j)}) d\mathbf{a}_{k,n-1}^{(j)}, \quad (32)$$

where the beliefs of the mobile agent state,  $q(\mathbf{x}_{n-1})$ , and of the PF states,  $\tilde{q}(\mathbf{a}_{k,n-1}^{(j)}, 1)$ , were calculated at the preceding time  $n-1$ . Inserting (6) and (7) for  $f(\tilde{\mathbf{a}}_{k,n}^{(j)}, \tilde{r}_{k,n}^{(j)} | \mathbf{a}_{k,n-1}^{(j)}, r_{k,n-1}^{(j)} = 1)$  and  $f(\tilde{\mathbf{a}}_{k,n}^{(j)}, \tilde{r}_{k,n}^{(j)} | \mathbf{a}_{k,n-1}^{(j)}, r_{k,n-1}^{(j)} = 0)$ , respectively, we obtain for  $r_{k,n}^{(j)} = 1$

$$\alpha_k(\tilde{\mathbf{a}}_{k,n}^{(j)}, 1) = P_s \int f(\tilde{\mathbf{a}}_{k,n}^{(j)} | \mathbf{a}_{k,n-1}^{(j)}) \tilde{q}(\mathbf{a}_{k,n-1}^{(j)}, 1) d\mathbf{a}_{k,n-1}^{(j)}, \quad (33)$$

and for  $r_{k,n}^{(j)} = 0$

$$\alpha_k^{(j)} = (1 - P_s) \int \tilde{q}(\mathbf{a}_{k,n-1}^{(j)}, 1) d\mathbf{a}_{k,n-1}^{(j)} + \tilde{q}_{k,n-1}^{(j)}, \quad (34)$$

where  $\alpha_k^{(j)} \triangleq \int \alpha_k(\mathbf{a}_{k,n}^{(j)}, 0) d\mathbf{a}_{k,n}^{(j)}$  and  $\tilde{q}_{k,n-1}^{(j)} \triangleq \int \tilde{q}(\mathbf{a}_{k,n-1}^{(j)}, 0) d\mathbf{a}_{k,n-1}^{(j)}$ .

After the prediction step, the following calculations are performed for all legacy PFs  $k \in \mathcal{K}_{n-1}^{(j)}$  and for all new PFs  $m \in \mathcal{M}_n^{(j)}$  for all PAs  $j \in \{1, \dots, J\}$  in parallel:

- 1) *Measurement evaluation for legacy PFs:* The messages  $\beta(c_{k,n}^{(j)})$  passed to the variable nodes corresponding to the feature-oriented DA variables  $c_{k,n}^{(j)}$  (cf. Fig. 2) are calculated as

$$\beta(c_{k,n}^{(j)}) = \int \int \alpha_k(\tilde{\mathbf{a}}_{k,n}^{(j)}, 1) \alpha(\mathbf{x}_n) g(\mathbf{x}_n, \tilde{\mathbf{a}}_{k,n}^{(j)}, 1, c_{k,n}^{(j)}; \mathbf{z}_n^{(j)}) d\mathbf{x}_n d\tilde{\mathbf{a}}_{k,n}^{(j)} + 1(c_{k,n}^{(j)}) \alpha_{k,n}^{(j)}. \quad (35)$$

- 2) *Measurement evaluation for new PFs:* The messages  $\xi(b_{m,n}^{(j)})$  passed to the variable nodes corresponding to the measurement-oriented DA variables  $b_{m,n}^{(j)}$  are calculated as

$$\xi(b_{m,n}^{(j)}) = \sum_{\check{r}_{m,n}^{(j)} \in \{0,1\}} \int \int h(\mathbf{x}_n, \check{\mathbf{a}}_{m,n}^{(j)}, \check{r}_{m,n}^{(j)}, b_{m,n}^{(j)}; \mathbf{z}_n^{(j)}) \alpha(\mathbf{x}_n) d\mathbf{x}_n d\check{\mathbf{a}}_{m,n}^{(j)}. \quad (36)$$

Inserting (24) for  $h(\mathbf{x}_n, \check{\mathbf{a}}_{m,n}^{(j)}, \check{r}_{m,n}^{(j)}, b_{m,n}^{(j)}; \mathbf{z}_n^{(j)})$ , this expression is easily seen to simplify to  $\xi(b_{m,n}^{(j)}) = 1$  for  $b_{m,n}^{(j)} \in \mathcal{K}_{n-1}^{(j)}$ , and for  $b_{m,n}^{(j)} = 0$  it becomes

$$\xi(b_{m,n}^{(j)}) = 1 + \frac{\mu_{n,n}^{(j)}}{\mu_{\text{FA}}^{(j)} f_{\text{FA}}(\mathbf{z}_{m,n}^{(j)})} \int \int \alpha(\mathbf{x}_n) f(\mathbf{z}_{m,n}^{(j)} | \mathbf{x}_n, \check{\mathbf{a}}_{m,n}^{(j)}) f_{n,n}(\check{\mathbf{a}}_n^{(j)} | \mathbf{x}_n) d\mathbf{x}_n d\check{\mathbf{a}}_{m,n}^{(j)}. \quad (37)$$

- 3) *Iterative data association:* Next, from  $\beta(c_{k,n}^{(j)})$  and  $\xi(b_{m,n}^{(j)})$ , messages  $\eta(c_{k,n}^{(j)})$  and  $\varsigma(b_{m,n}^{(j)})$  are obtained through a loopy (iterative) BP scheme. First, for each measurement  $m \in \mathcal{M}_n^{(j)}$ , messages  $\nu_{m \rightarrow k}^{(p)}(c_{k,n}^{(j)})$  and  $\zeta_{k \rightarrow m}^{(p)}(b_{m,n}^{(j)})$  are calculated iteratively according to [36], [39]

$$\nu_{m \rightarrow k}^{(p)}(c_{k,n}^{(j)}) = \sum_{b_{m,n}^{(j)} = 0}^{K_{n-1}^{(j)}} \xi(b_{m,n}^{(j)}) \psi(c_{k,n}^{(j)}, b_{m,n}^{(j)}) \prod_{k' \in \mathcal{K}_{n-1}^{(j)} \setminus \{k\}} \zeta_{k' \rightarrow m}^{(p-1)}(b_{m,n}^{(j)}) \quad (38)$$

$$\zeta_{k \rightarrow m}^{(p)}(b_{m,n}^{(j)}) = \sum_{c_{k,n}^{(j)}=0}^{M_n^{(j)}} \beta(c_{k,n}^{(j)}) \psi(c_{k,n}^{(j)}, b_{m,n}^{(j)}) \prod_{m' \in \mathcal{M}_n^{(j)} \setminus \{m\}} \nu_{m' \rightarrow k}^{(p)}(c_{k,n}^{(j)}), \quad (39)$$

for  $k = 1, \dots, K_{n-1}^{(j)}$ ,  $m = 1, \dots, M_n^{(j)}$ , and iteration index  $p = 1, \dots, P$ . The recursion defined by (38) and (39) is initialized (for  $p=0$ ) by  $\zeta_{k \rightarrow m}^{(0)}(b_{m,n}^{(j)}) = \sum_{c_{k,n}^{(j)}=0}^{M_n^{(j)}} \beta(c_{k,n}^{(j)}) \psi(c_{k,n}^{(j)}, b_{m,n}^{(j)})$ . Then, after the last iteration  $p = P$ , the messages  $\eta(c_{k,n}^{(j)})$  and  $\varsigma(b_{m,n}^{(j)})$  are calculated as

$$\eta(c_{k,n}^{(j)}) = \prod_{m \in \mathcal{M}_n^{(j)}} \nu_{m \rightarrow k}^{(P)}(c_{k,n}^{(j)}), \quad \varsigma(b_{m,n}^{(j)}) = \prod_{k \in \mathcal{K}_{n-1}^{(j)}} \zeta_{k \rightarrow m}^{(P)}(b_{m,n}^{(j)}). \quad (40)$$

4) *Measurement update for the agent*: From  $\eta(c_{k,n}^{(j)})$ ,  $\alpha_k(\tilde{\mathbf{a}}_{k,n}^{(j)}, 1)$ , and  $\alpha_{k,n}^{(j)}$ , the message  $\gamma_k^{(j)}(\mathbf{x}_n)$  related to the agent is calculated as

$$\gamma_k^{(j)}(\mathbf{x}_n) = \sum_{c_{k,n}^{(j)}=0}^{M_n^{(j)}} \eta(c_{k,n}^{(j)}) \int \alpha_k(\tilde{\mathbf{a}}_{k,n}^{(j)}, 1) g(\mathbf{x}_n, \tilde{\mathbf{a}}_{k,n}^{(j)}, 1, c_{k,n}^{(j)}; \mathbf{z}_n^{(j)}) d\tilde{\mathbf{a}}_{k,n}^{(j)} + \eta(c_{k,n}^{(j)}=0) \alpha_{k,n}^{(j)}. \quad (41)$$

5) *Measurement update for legacy PFs*: Similarly, the messages  $\gamma(\tilde{\mathbf{a}}_{k,n}^{(j)}, \tilde{r}_{k,n}^{(j)})$  related to the legacy PFs are calculated as

$$\gamma(\tilde{\mathbf{a}}_{k,n}^{(j)}, 1) = \sum_{c_{k,n}^{(j)}=0}^{M_n^{(j)}} \eta(c_{k,n}^{(j)}) \int \alpha(\mathbf{x}_n) g(\mathbf{x}_n, \tilde{\mathbf{a}}_{k,n}^{(j)}, 1, c_{k,n}^{(j)}; \mathbf{z}_n^{(j)}) d\mathbf{x}_n \quad (42)$$

$$\gamma_{k,n}^{(j)} \triangleq \gamma(\tilde{\mathbf{a}}_{k,n}^{(j)}, 0) = \eta(c_{k,n}^{(j)}=0). \quad (43)$$

6) *Measurement update for new PFs*: Finally, the messages  $\phi(\check{\mathbf{a}}_{m,n}^{(j)}, \check{r}_{m,n}^{(j)})$  related to the new PFs are calculated as

$$\phi(\check{\mathbf{a}}_{m,n}^{(j)}, 1) = \varsigma(b_{m,n}^{(j)}=0) \int \alpha(\mathbf{x}_n) h(\mathbf{x}_n, \check{\mathbf{a}}_{m,n}^{(j)}, 1, 0; \mathbf{z}_n^{(j)}) d\mathbf{x}_n \quad (44)$$

$$\phi_{m,n}^{(j)} \triangleq \phi(\check{\mathbf{a}}_{m,n}^{(j)}, 0) = \sum_{b_{m,n}^{(j)}=0}^{K_{n-1}^{(j)}} \varsigma(b_{m,n}^{(j)}). \quad (45)$$

Once these messages are available, the beliefs approximating the desired marginal posterior pdfs are obtained. The belief for the agent state is given, up to a normalization factor, by

$$q(\mathbf{x}_n) \propto \alpha(\mathbf{x}_n) \prod_{j=1}^J \prod_{k \in \mathcal{K}_{n-1}^{(j)}} \gamma_k^{(j)}(\mathbf{x}_n). \quad (46)$$

This belief after normalization provides an approximation of the marginal posterior pdf  $f(\mathbf{x}_n | \mathbf{z}_{1:n})$ , and it is used instead of  $f(\mathbf{x}_n | \mathbf{z}_{1:n})$  in (27). Furthermore, the beliefs  $\tilde{q}(\tilde{\mathbf{a}}_{k,n}^{(j)}, \tilde{r}_{k,n}^{(j)})$

for the augmented states of the legacy PFs,  $\tilde{\mathbf{y}}_{k,n}^{(j)} = [\tilde{\mathbf{a}}_{k,n}^{(j)\top} \tilde{r}_{k,n}^{(j)}]^\top$ , are calculated as

$$\tilde{q}(\tilde{\mathbf{a}}_{k,n}^{(j)}, 1) \propto \alpha_k(\tilde{\mathbf{a}}_{k,n}^{(j)}, 1) \gamma(\tilde{\mathbf{a}}_{k,n}^{(j)}, 1), \quad \tilde{q}_{k,n}^{(j)} \triangleq \tilde{q}(\tilde{\mathbf{a}}_{k,n}^{(j)}, 0) \propto \alpha_{k,n}^{(j)} \gamma_{k,n}^{(j)}, \quad (47)$$

and the beliefs  $\check{q}(\check{\mathbf{a}}_{m,n}^{(j)}, \check{r}_{m,n}^{(j)})$  for the augmented states of the new PFs,  $\check{\mathbf{y}}_{m,n}^{(j)} = [\check{\mathbf{a}}_{m,n}^{(j)\top} \check{r}_{m,n}^{(j)}]^\top$ , as

$$\check{q}(\check{\mathbf{a}}_{m,n}^{(j)}, 1) \propto \phi(\check{\mathbf{a}}_{m,n}^{(j)}, 1), \quad \check{q}_{m,n}^{(j)} \triangleq \check{q}(\check{\mathbf{a}}_{m,n}^{(j)}, 0) \propto \phi_{m,n}^{(j)}. \quad (48)$$

In particular,  $\tilde{q}(\tilde{\mathbf{a}}_{k,n}^{(j)}, 1)$  and  $\check{q}(\check{\mathbf{a}}_{m,n}^{(j)}, 1)$  approximate the marginal posterior pdf  $f(\mathbf{a}_{k',n}^{(j)}, r_{k',n}^{(j)} = 1 | \mathbf{z}_{1:n})$ , where  $k' \in \mathcal{K}_{n-1}^{(j)} \cup \mathcal{M}_n^{(j)}$  (assuming an appropriate index mapping between  $k$  and  $m$  on the one hand and  $k'$  on the other), and they are used in (28) and (29), (30).

An exact calculation of the various messages and beliefs presented above is infeasible. An efficient approximate calculation can be based on the sequential Monte Carlo (particle-based) implementation approach introduced in [38], [49]. In our case, the sequential Monte Carlo implementation uses a “stacked state” [49] comprising the agent state and the PF states. The resulting complexity scales only linearly in the number of particles. A flowchart and a MATLAB implementation of the proposed algorithm are available online at <https://gitlab.com/erikleitinger/BP-Multipath-basedSLAM>.

## VI. STATE PROPAGATION FOR UNDETECTED FEATURES

In parallel to, and in support of, the BP-based detection and estimation algorithm, we use a “zero-measurement” PHD filter in order to propagate information about features that potentially exist but did not generate any measurement yet. Such features will be termed *undetected features* in what follows. A similar strategy was previously introduced in the context of MTT [32], [42]. This propagation of information about undetected features enables the calculation of the intensity function of newly detected features,  $\lambda_n^n(\mathbf{a}_{:,n}^{(j)} | \mathbf{x}_n) = \mu_{n,n}^{(j)} f_{n,n}(\mathbf{a}_{:,n}^{(j)} | \mathbf{x}_n)$ , for all PAs  $j$  at time  $n$ . Note that  $\lambda_n^n(\check{\mathbf{a}}_{m,n}^{(j)} | \mathbf{x}_n)$  occurs in  $h(\mathbf{x}_n, \check{\mathbf{a}}_{m,n}^{(j)}, 1, 0; \mathbf{z}_n^{(j)})$  in (24), which is needed in the measurement evaluation and measurement update steps for new PFs (see Section V-B). We will first review the concept of a Poisson random finite set (RFS), which underlies the PHD filter.

### A. RFS Basics

An RFS [33], also known as a simple finite point process [50], is a set-valued random variable  $\mathsf{X} = \{\mathbf{x}^{(1)}, \dots, \mathbf{x}^{(k)}\}$ . The elements of  $\mathsf{X}$  are random vectors  $\mathbf{x}^{(i)} \in \mathbb{R}^{N_x}$ ; they are unordered and their number  $k = |\mathsf{X}| \in \mathbb{N}_0$ —i.e., the cardinality of  $\mathsf{X}$ —is random. The realizations of  $\mathsf{X}$ ,  $\mathcal{X} = \{\mathbf{x}^{(1)}, \dots, \mathbf{x}^{(k)}\}$ , are finite sets of vectors  $\mathbf{x}^{(1)}, \dots, \mathbf{x}^{(k)} \in \mathbb{R}^{N_x}$ . Within the FISST

framework [33], an RFS  $X$  can be described by its pdf  $f_X(\mathcal{X})$ , briefly denoted  $f(\mathcal{X})$ . The pdf evaluated for a realization  $\mathcal{X} = \{\mathbf{x}^{(1)}, \dots, \mathbf{x}^{(k)}\}$  is given by  $f(\mathcal{X}) = f(\{\mathbf{x}^{(1)}, \dots, \mathbf{x}^{(k)}\}) = k! \rho(k) f_k(\mathbf{x}^{(1)}, \dots, \mathbf{x}^{(k)})$ . Here,  $\rho(k) \triangleq \Pr\{|\mathcal{X}| = k\}$  is the pmf of the cardinality  $k = |\mathcal{X}|$ , which is termed the cardinality distribution, and  $f_k(\mathbf{x}^{(1)}, \dots, \mathbf{x}^{(k)})$  is the joint pdf of the random vectors  $\mathbf{x}^{(1)}, \dots, \mathbf{x}^{(k)}$ , which is required to be invariant to a permutation of its arguments  $\mathbf{x}^{(i)}$ .

An important special RFS is the Poisson RFS. The elements of a Poisson RFS  $X$  are iid with some ‘‘spatial pdf’’  $f(\mathbf{x})$ . Thus, for cardinality  $|\mathcal{X}| = k$ ,  $f_k(\mathbf{x}^{(1)}, \dots, \mathbf{x}^{(k)}) = \prod_{i=1}^k f(\mathbf{x}^{(i)}) = \prod_{\mathbf{x} \in \mathcal{X}} f(\mathbf{x})$ . The cardinality  $k = |\mathcal{X}|$  is Poisson distributed, i.e.,  $\rho(k) = e^{-\mu} \mu^k / k!$ ,  $k \in \mathbb{N}_0$ , where  $\mu$  is the mean of  $k$ . The pdf of  $X$  follows as  $f(\mathcal{X}) = e^{-\mu} \prod_{\mathbf{x} \in \mathcal{X}} \mu f(\mathbf{x})$ . The Poisson RFS is also fully characterized by its intensity function or PHD, which is given by  $\lambda(\mathbf{x}) = \mu f(\mathbf{x})$ .

### B. Zero-Measurement PHD Filter

The PHD filter is a popular technique for tracking an RFS [33]. In the PHD filter, the state is modeled as a Poisson RFS. The original PHD filter [33] propagates the intensity functions of both the detected and undetected features. To keep the RFS within the class of Poisson RFSs, an approximation based on the minimization of a Kullback-Leibler divergence is performed in the update step of the PHD filter [33]. In [32], [42], a PHD filter that propagates only the intensity function of the undetected features is introduced. In this filter, which we will term a zero-measurement PHD filter, the propagated RFS remains within the class of Poisson RFSs without any approximation. In the proposed SLAM algorithm, the zero-measurement PHD filter complements the BP-based algorithm in Section V-B because it propagates information about undetected features whereas the BP-based algorithm propagates information about detected features. We assume that at the initial time  $n = 1$ , the state of the undetected features for PA  $j$  is a Poisson RFS with intensity function  $\lambda^u(\mathbf{a}_{:,1}^{(j)})$ . If no prior information on the spatial distribution of VAs and PAs is incorporated,  $\lambda^u(\mathbf{a}_{:,1}^{(j)})$  is constant on the region of interest (ROI), with the integral of  $\lambda^u(\mathbf{a}_{:,1}^{(j)})$  over the ROI chosen equal to the expected number of features in the ROI. Using a zero-measurement PHD filter, state propagation for the undetected features amounts to propagating the intensity function of the Poisson RFS (i.e.,  $\lambda^u(\mathbf{a}_{:,n-1}^{(j)}) \rightarrow \lambda^u(\mathbf{a}_{:,n}^{(j)})$ ). This propagation consists of a prediction step and an update step.

1) *Prediction Step:* In the prediction step, which is identical to that of the original PHD filter [33], the preceding intensity function  $\lambda^u(\mathbf{a}_{:,n-1}^{(j)})$  is converted into a ‘‘predicted intensity

function”  $\lambda_{n|n-1}^u(\mathbf{a}_{:,n}^{(j)})$  according to

$$\lambda_{n|n-1}^u(\mathbf{a}_{:,n}^{(j)}) = P_s \int f(\mathbf{a}_{:,n}^{(j)} | \mathbf{a}_{:,n-1}^{(j)}) \lambda_{n-1}^u(\mathbf{a}_{:,n-1}^{(j)}) d\mathbf{a}_{:,n-1}^{(j)} + \lambda^b(\mathbf{a}_{:,n}^{(j)}), \quad (49)$$

where  $f(\mathbf{a}_{:,n}^{(j)} | \mathbf{a}_{:,n-1}^{(j)})$  is the state-transition pdf of the undetected feature state. Here,  $\lambda^b(\mathbf{a}_{:,n}^{(j)})$  is the intensity function of a Poisson RFS that models the birth of new features. In the SLAM context, it may be reasonable to set  $\lambda^b(\mathbf{a}_{:,n}^{(j)}) = 0$ , which expresses the assumption that the indoor geometry does not change during the mapping process. From  $\lambda_{n|n-1}^u(\mathbf{a}_{:,n}^{(j)})$ , the conditional pdf  $f_{n,n}(\mathbf{a}_{:,n}^{(j)} | \mathbf{x}_n)$  for newly detected features for PA  $j$  is obtained as [32]

$$f_{n,n}(\mathbf{a}_{:,n}^{(j)} | \mathbf{x}_n) = \frac{P_d^{(j)}(\mathbf{x}_n, \mathbf{a}_{:,n}^{(j)}) \lambda_{n|n-1}^u(\mathbf{a}_{:,n}^{(j)})}{\int P_d^{(j)}(\mathbf{x}_n, \mathbf{a}_{:,n}^{(j)'}) \lambda_{n|n-1}^u(\mathbf{a}_{:,n}^{(j)'}) d\mathbf{a}_{:,n}^{(j)'}}, \quad (50)$$

where  $P_d^{(j)}(\mathbf{x}_n, \mathbf{a}_{:,n}^{(j)})$  is the detection probability of the undetected feature state for PA  $j$ . Furthermore, the mean number of newly detected features is given by  $\mu_{n,n}^{(j)} = \int \int P_d^{(j)}(\mathbf{x}_n, \mathbf{a}_{:,n}^{(j)}) \times \lambda_{n|n-1}^u(\mathbf{a}_{:,n}^{(j)}) \alpha(\mathbf{x}_n) d\mathbf{a}_{:,n}^{(j)} d\mathbf{x}_n$ , with  $\alpha(\mathbf{x}_n)$  according to (31). As mentioned earlier,  $f_{n,n}(\mathbf{a}_{:,n}^{(j)} | \mathbf{x}_n)$  and  $\mu_{n,n}^{(j)}$  are needed in the measurement evaluation and measurement update steps for new PFs described in Section V-B.

2) *Update Step*: In the update step, the predicted intensity function  $\lambda_{n|n-1}^u(\mathbf{a}_{:,n}^{(j)})$  is converted into the new (updated) intensity function  $\lambda^u(\mathbf{a}_{:,n}^{(j)})$  according to [32], [42]

$$\lambda^u(\mathbf{a}_{:,n}^{(j)}) = (1 - P_d^{(j)}(\mathbf{a}_{:,n}^{(j)})) \lambda_{n|n-1}^u(\mathbf{a}_{:,n}^{(j)}), \quad (51)$$

where  $P_d^{(j)}(\mathbf{a}_{:,n}^{(j)}) = \int P_d^{(j)}(\mathbf{x}_n, \mathbf{a}_{:,n}^{(j)}) \alpha(\mathbf{x}_n) d\mathbf{x}_n$ . We note that this update relation is identical to that of the original PHD filter [33] for the case where no measurements are available. The intensity function  $\lambda^u(\mathbf{a}_{:,n}^{(j)})$  represents essentially “negative information” in the sense that for  $\lambda^b(\mathbf{a}_{:,n}^{(j)}) = 0$ ,  $\lambda^u(\mathbf{a}_{:,n}^{(j)})$  is high in those parts of the ROI that have not been explored by the mobile agent yet, and for  $\lambda^b(\mathbf{a}_{:,n}^{(j)}) > 0$ , it is high in those parts of the ROI that have not been explored for some time. The expressions (49) and (51) are calculated by using a sequential Monte Carlo implementation, similarly to [43].

## VII. EXPERIMENTAL RESULTS

To analyze the performance of the proposed algorithm, we apply it to synthetic and real measurement data within two-dimensional (2-D) scenarios. The parameters involved in the algorithm and those used to generate the synthetic measurements are listed in Table I.

TABLE I: Simulation parameters.

| Parameters involved in the proposed algorithm |  |                    |            |                         |                  |             |       |             |                  |                   |  |            |
|---|--|--------------------|------------|-------------------------|------------------|-------------|-------|-------------|------------------|-------------------|--|------------|
| $\sigma_w$                                    | $\sigma_a$                                     | $\sigma_{a,1}$     | $\sigma_m$ | $\mu_{\text{FA}}^{(j)}$ | $\mu_b$          | $\mu_{n,1}$ | $P_s$ | $P_d$       | $P_{\text{det}}$ | $P_{\text{prun}}$ | #particles                             | #simu.runs |
| 0.01 m/s <sup>2</sup>                         | 10 <sup>-4</sup> m or 0.5 · 10 <sup>-2</sup> m | 10 <sup>-3</sup> m | 0.15 m     | 1 or 2                  | 10 <sup>-4</sup> | 6           | 0.999 | 0.95 or 0.5 | 0.5              | 10 <sup>-4</sup>  | 10 <sup>5</sup> or 3 · 10 <sup>4</sup> | 100 or 30  |

| Parameters used to generate the synthetic measurements |             |                      |
|--|-------------|----------------------|
| $\mu_{\text{FA}}^{(j)}$                                | $P_d$       | $\sigma_{m,n}^{(j)}$ |
| 1 or 2   | 0.95 or 0.5 | 0.1 m                |

### A. Analysis Setup

1) *State-Evolution Model*: The agent's state-transition pdf  $f(\mathbf{x}_n|\mathbf{x}_{n-1})$ , with  $\mathbf{x}_n = [\mathbf{p}_n^T \mathbf{v}_n^T]^T$ , is defined by a linear, near constant-velocity motion model [51, Sec. 6.3.2], i.e.,

$$\mathbf{x}_n = \begin{bmatrix} 1 & 0 & \Delta T & 0 \\ 0 & 1 & 0 & \Delta T \\ 0 & 0 & 1 & 0 \\ 0 & 0 & 0 & 1 \end{bmatrix} \mathbf{x}_{n-1} + \begin{bmatrix} \Delta T^2/2 & 0 \\ 0 & \Delta T^2/2 \\ \Delta T & 0 \\ 0 & \Delta T \end{bmatrix} \mathbf{w}_n. \quad (52)$$

Here,  $\Delta T = 1$  s and the driving process  $\mathbf{w}_n$  is independent across  $n$ , zero-mean, and Gaussian with covariance matrix  $\mathbf{Q}_w = \sigma_w^2 \mathbf{I}_2$ , where  $\mathbf{I}_2$  denotes the  $2 \times 2$  identity matrix. The PFs are static, i.e., the state-transition pdfs are given by  $f(\tilde{\mathbf{a}}_{k,n}^{(j)}|\mathbf{a}_{k,n-1}^{(j)}) = \delta(\tilde{\mathbf{a}}_{k,n}^{(j)} - \mathbf{a}_{k,n-1}^{(j)})$ , where  $\delta(\cdot)$  is the Dirac delta function. However, in our implementation of the proposed algorithm, we introduced a small driving process in the PF state-evolution model for the sake of numerical stability. Accordingly, the state evolution is modeled as  $\tilde{\mathbf{a}}_{k,n}^{(j)} = \mathbf{a}_{k,n-1}^{(j)} + \boldsymbol{\omega}_{k,n}^{(j)}$ , where  $\boldsymbol{\omega}_{k,n}^{(j)}$  is independent across  $k$ ,  $n$ , and  $j$ , zero-mean, and Gaussian with covariance matrix  $\boldsymbol{\Omega}_{k,n}^{(j)} = \sigma_a^2 \mathbf{I}_2$ .

2) *Measurement Model*: In contrast to usual SLAM setups [2], our measurement model is solely based on MPC ranges, i.e., it does not exploit bearing information or information derived from inertial measurement unit sensors. The scalar range measurements  $z_{m,n}^{(j)}$  are modeled as

$$z_{m,n}^{(j)} = \|\mathbf{p}_n - \mathbf{a}_{k,n}^{(j)}\| + \nu_{m,n}^{(j)}, \quad (53)$$

where the measurement noise  $\nu_{m,n}^{(j)}$  is independent across  $m$ ,  $n$ , and  $j$ , zero-mean, and Gaussian with variance  $\sigma_{m,n}^{(j)2}$ . The measurement model (53) determines the likelihood function factors  $f(z_{m,n}^{(j)}|\mathbf{x}_n, \tilde{\mathbf{a}}_{k,n}^{(j)})$  and  $f(z_{m,n}^{(j)}|\mathbf{x}_n, \tilde{\mathbf{a}}_{m,n}^{(j)})$  in (14). However, we emphasize that our proposed SLAM algorithm can be extended to measurement models that include bearing measurements (AoAs and/or AoDs) or measurements from inertial measurement unit sensors. Such an extension would further improve the robustness of our approach.

3) *Common Simulation Parameters:* The following implementation parameters are used for both synthetic and real measurements, see also Table I. (Parameters that are chosen differently will be described in Sections VII-B and VII-C.) We use the floor plan shown in Fig. 1, with two static PAs at positions  $\mathbf{a}_{1,n}^{(1)}$  and  $\mathbf{a}_{1,n}^{(2)}$ . The false alarm pdf  $f_{\text{FA}}(z_{m,n}^{(j)})$  is uniform on  $[0\text{m}, 30\text{m}]$ . The birth intensity function  $\lambda^b(\mathbf{a}_{:,n}^{(j)})$  is uniform on the ROI, which is a circular disk of radius 30m around the center of the floor plan shown in Fig. 1. Thus,  $\lambda^b(\mathbf{a}_{:,n}^{(j)}) = \mu_b / (2\pi(30\text{m})^2)$ . Similarly, the initial undetected feature intensity is uniform on the ROI, i.e.,  $\lambda_1^u(\mathbf{a}_{:,1}^{(j)}) = \mu_{n,1}^{(j)} / (2\pi(30\text{m})^2)$ . The values of the parameters  $\mu_b$ ,  $\mu_{n,1}^{(j)}$ ,  $\sigma_w$ ,  $\sigma_a$ ,  $P_s$ ,  $P_{\text{det}}$ , and  $P_{\text{prun}}$  are given in Table I.

Our implementation of the proposed algorithm uses a sequential importance resampling particle filter scheme that follows the implementations in [38], [49]. The particles for the initial states of the two PAs are drawn from the 2-D Gaussian distributions  $\mathcal{N}(\mathbf{a}_{1,1}^{(j)}, \sigma_{a,1}^2 \mathbf{I}_2)$ , where  $\mathbf{a}_{1,1}^{(j)}$  is the position of PA  $j \in \{1, 2\}$  and  $\sigma_{a,1} = 0.001\text{m}$ . This highly informative prior implies that the initial PA positions are effectively known. The particles for the initial agent state are drawn from a 4-D uniform distribution with center  $\mathbf{x}_1 = [\mathbf{p}_1^T \ 0 \ 0]^T$ , where  $\mathbf{p}_1$  is the starting position of the agent trajectory, and with the support of each component about the respective center given by  $[-0.5, 0.5]$  (in m for the position and m/s for the velocity). We note that our algorithm would still perform well without any prior information about the initial states of the mobile agent and the PAs. However, because it uses only relative range measurements, the estimated feature map and agent trajectory would then contain an arbitrary translation and rotation relative to the true positions. Finally, the number  $P$  of message passing iterations for DA is limited by the termination condition  $[\sum_{k \in \mathcal{K}_{n-1}^{(j)}} \sum_{m \in \mathcal{M}_n^{(j)}} (\nu_{m \rightarrow k}^{(p)}(c_{k,n}^{(j)}) - \nu_{m \rightarrow k}^{(p-1)}(c_{k,n}^{(j)}))^2]^{1/2} < 10^{-7}$  (cf. (38)) or by the maximum number  $P_{\text{max}} = 1000$ .

### B. Results for Synthetic Measurements

For our simulations based on synthetic measurements, we used the common simulation parameters described above. The range measurements were generated with a measurement noise standard deviation  $\sigma_{m,n}^{(j)} = 0.1\text{m}$ . However, for numerical robustness, the algorithm used a measurement noise standard deviation  $\sigma_m = 1.5 \cdot \sigma_{m,n}^{(j)}$ . The standard deviation of the driving process in the PF state-evolution model was  $\sigma_a = 10^{-4}\text{m}$ . We considered three different parameter settings dubbed SLAM 1, SLAM 2, and SLAM 3. In SLAM 1 and SLAM 2, we used detection probability  $P_d^{(j)}(\mathbf{x}_n, \mathbf{a}_{k,n}^{(j)}) = P_d = 0.95$  and mean number of false alarms  $\mu_{\text{FA}}^{(j)} = 1$ . The posterior pdfs of the state of the mobile agent, of the states of legacy PFs, and of the states of new PFs were each

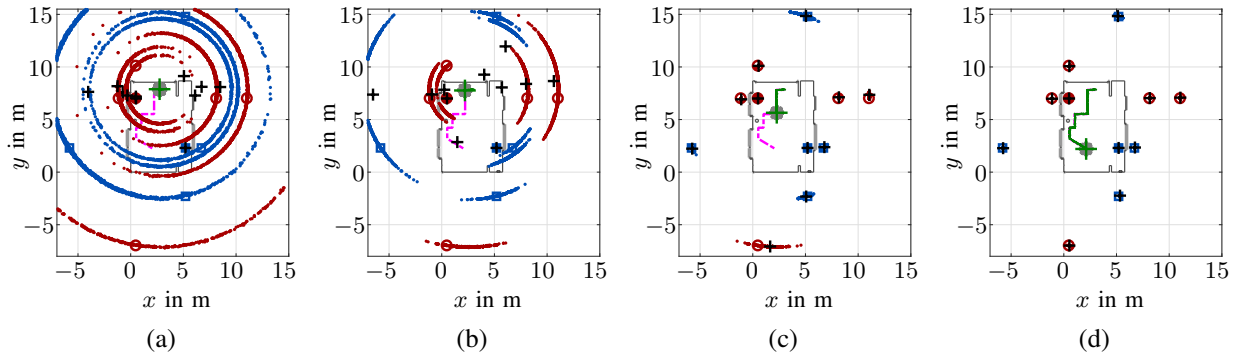


Fig. 3: Particle convergence. Particles representing the posterior pdfs of the state of the mobile agent (gray) and of the states of the detected PFs (red for PA 1, blue for PA 2) are shown at (a)  $n = 30$ , (b)  $n = 90$ , (c)  $n = 300$ , and (d)  $n = 900$ . The positions of PA 1 and PA 2 are indicated by a red bullet and a blue box, respectively, and the corresponding geometrically expected VA positions by red circles and blue squares. The green line represents the MMSE estimates of the mobile agent position, and the green cross the MMSE estimate of the currently last mobile agent position. The black crosses indicate the MMSE estimates of the positions of the detected PFs.

represented by 100.000 (SLAM 1) or by 30.000 (SLAM 2) particles.<sup>1</sup> In SLAM 3, we used  $P_d = 0.5$  and  $\mu_{FA}^{(j)} = 2$  to analyze the robustness of the proposed algorithm to extremely poor radio signal conditions, i.e., to scenarios characterized by a high probability that existing MPCs are not detected or nonexisting MPCs are detected; for this parameter setting, the agent state and the PF states were each represented by 100.000 particles. We performed 100 simulation runs. In each simulation run, we generated with detection probability  $P_d$  noisy ranges  $z_{m,n}^{(j)}$  according to (53). Evaluation of (53) was based on the fixed PA positions  $\mathbf{a}_{1,n}^{(1)}$ ,  $\mathbf{a}_{1,n}^{(2)}$  and the fixed VA positions  $\mathbf{a}_{l,n}^{(j)} \in \mathbb{R}^2$ ,  $l = 2, \dots, L_n^{(j)}$  for  $j = 1, 2$  (shown in Fig. 1), where  $L_n^{(1)} = 6$  and  $L_n^{(2)} = 5$  are the numbers of features (PA plus VAs). In addition, false alarm measurements  $z_{m,n}^{(j)}$  were generated according to the false alarm parameters described above.

For one exemplary simulation run, Fig. 3 illustrates the convergence of the posterior pdfs of the PF positions to the true feature (PA and VA) positions by displaying the respective particles at times  $n = 30, 90, 300, 900$ . These results demonstrate that the proposed algorithm is able to cope with highly multimodal distributions and with measurements conveying only very limited information at each time step (since only range measurements are used).

Fig. 4 shows the root mean square error (RMSE) of the estimated time-varying agent position,

<sup>1</sup>The number of particles could be strongly reduced if, e.g., the MPCs' AoAs were used in addition to the range measurements, since this would decrease the effective support regions of the posterior pdfs. The number of particles could also be reduced by performing an adaptive adjustment of the detection probability  $P_d$  as in [28]. However, since the complexity of the proposed algorithm scales only linearly with the number of particles, the runtime of a MATLAB implementation on an Intel i7-6820HQ CPU is still below 0.4s per time step  $n$  even for the high numbers of particles we are using.

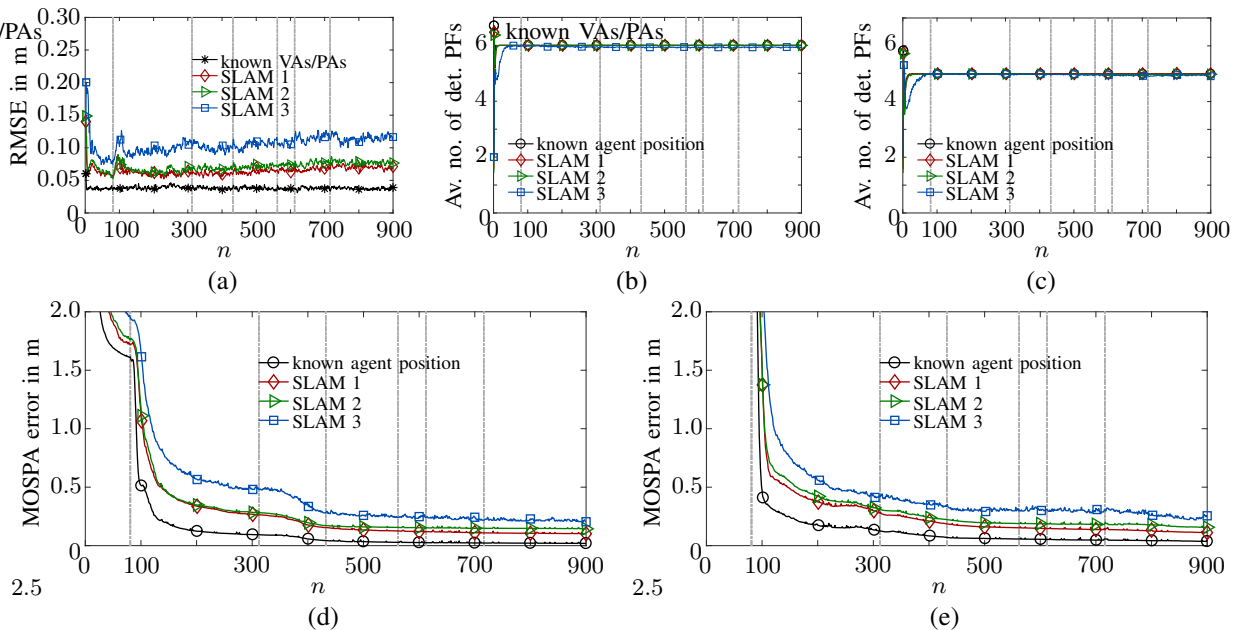


Fig. 4: Results for synthetic measurements: (a) Average agent position RMSE, (b) and (c) average number of detected PFs associated with PA 1 and 2, respectively, (d) and (e) MOSPA error for, respectively, PA 1 and 2 and the associated VAs. The curves labeled “known agent position” show the performance for the case where the agent position is known. Note that in (b) and (c) the curves labeled “known agent position,” “SLAM 1,” and “SLAM 2” coincide. The vertical dash-dotted lines indicate the times around which the mobile agent performs turns.

the average numbers of detected PFs for the two PAs, and the mean optimal subpattern assignment (MOSPA)<sup>2</sup> errors [52] for the two PAs and the associated VAs, all versus time  $n$ . These results were obtained by averaging over the 100 simulation runs. The MOSPA errors are based on the Euclidean metric and use cutoff parameter 5m and order parameter 1 [52]. It can be seen in Fig. 4(a) that the average agent position RMSE is mostly below 0.12m for all parameters settings and below 0.073m for SLAM 1 and SLAM 2. The average numbers of detected PFs in Figs. 4(b), (c) are seen to be effectively equal to the respective true numbers of features  $L_n^{(1)} = 6$  and  $L_n^{(2)} = 5$  for SLAM 1 and SLAM 2. For SLAM 3, the average numbers are slightly below the true numbers, which can be explained by the low detection probability  $P_d = 0.5$  and the high mean number of false alarms  $\mu_{FA}^{(j)} = 2$  relative to the true numbers of features. However, the performance of the algorithm is still good, which suggests that the algorithm has a high level of robustness. The MOSPA errors for SLAM 1 are seen in Figs. 4(d), (e) to decrease with time until they are ultimately below 0.11m for both PAs. The position RMSEs of the individual PFs

<sup>2</sup>We remark that an alternative to the “classical” OSPA metric [52] is provided by the generalized OSPA metric proposed in [53], which does not normalize the OSPA error by the cardinality of the larger set and penalizes the cardinality error differently.

are at most 0.25m and in many cases around 0.05m. In general, the RMSE and MOSPA errors for SLAM 2 and SLAM 3 are slightly larger (ultimately 0.15m for SLAM 2 and 0.20m for SLAM 3).

As a performance benchmark for the accuracy of agent localization, we compare in Fig. 4(a) the average agent position RMSE of the proposed algorithm to that of the algorithm in [7], which also uses BP-based probabilistic DA but assumes knowledge of the feature map, i.e., of the PA/VA positions. In addition, as a performance benchmark for the accuracy of feature map estimation, we compare in Figs. 4(b)–(e) the average number of detected PFs and the MOSPA errors to those that would be obtained for the SLAM 1 parameter setting if the agent position was known at all times. These benchmarks provide bounds on the two main performance aspects of SLAM, i.e., accuracy in localization and mapping.<sup>3</sup>

### C. Results for Real Measurements

For experiments using real measurements, we chose  $P_d^{(j)}(\mathbf{x}_n, \mathbf{a}_{k,n}^{(j)}) = P_d = 0.6$  and  $\mu_{\text{FA}}^{(j)} = 2$ . This accounts for the fact that the diffuse multipath existing in indoor environments causes the preliminary signal analysis stage to detect features with a lower probability and to produce false alarms with a higher probability. The measurements were taken from the seminar room scenario previously used in [28], [55]. They correspond to five closely spaced parallel trajectories each consisting of 900 agent positions with a spacing of 0.01m, resulting in a total number of 4500 agent positions. The magenta line in Fig. 1 represents one of the five trajectories. Note that in our simulations, each individual trajectory is processed independently, i.e., the estimated PF positions of a trajectory are not used as prior knowledge for another trajectory. More details about the measurements can be found in [55]. At each agent position, the agent transmitted an ultra-wideband signal, which was received by the two static PAs. This signal was measured using an M-sequence correlative channel sounder with frequency range 3–10GHz and antennas with an approximately uniform radiation pattern in the azimuth plane and zeros in the floor and ceiling directions. Within the measured band, the actual signal band was selected by a filter with raised-cosine impulse response  $s(t)$  with a roll-off factor of 0.5, a two-sided 3-dB bandwidth of 2GHz,

<sup>3</sup>We note that it was previously shown [15] that algorithms that assume independence of the feature states and use probabilistic DA (e.g., Rao-Blackwellized SLAM [1], [15]) are more accurate and robust and also less complex than algorithms that estimate the feature states jointly but do not use probabilistic DA (e.g., EKF-SLAM [13]), especially for heavily cluttered measurements. It was also shown in [14] that RFS-based Rao-Blackwellized SLAM algorithms exhibit a better performance and a lower complexity than algorithms that combine joint estimation of the feature states with multiple hypothesis tracking (e.g., [54]). Therefore, we do not present performance comparisons with such algorithms.

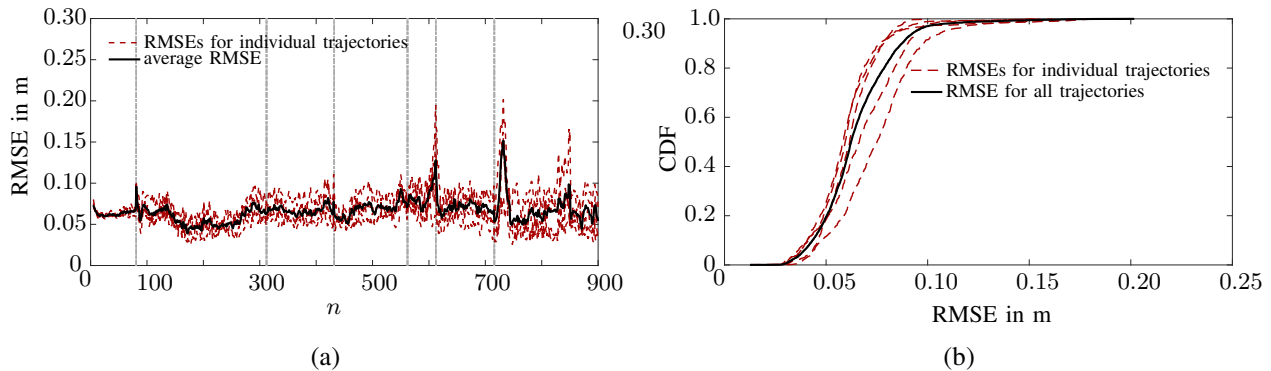


Fig. 5: Results for real measurements: (a) Agent position RMSEs for the five individual trajectories and average RMSE (averaged over the five trajectories), (b) empirical CDFs of the RMSEs for the five individual trajectories and empirical CDF of the five RMSEs taken together.

and a center frequency of 7GHz. From the measured signals, the range measurements  $z_{m,n}^{(j)} = c\hat{\tau}_{m,n}^{(j)}$  constituting the input to the proposed algorithm were derived by means of a snapshot-based SISO SAGE algorithm [22] for estimating the delays  $\hat{\tau}_{m,n}^{(j)}$  and complex amplitudes  $\hat{\alpha}_{m,n}^{(j)}$  of the MPCs (cf. (1)). In this method, the maximum number of estimated MPCs for each PA  $j$  was defined as  $M_{n,\max}^{(j)} = 20$ . Estimates of the range variances  $\hat{\sigma}_{m,n}^{(j)2}$  (cf. (53)) were determined from the estimated complex amplitudes as described in [28], [55]. The standard deviation of the driving process in the PF state-evolution model was  $\sigma_a = 0.5 \cdot 10^{-2}$  m. We performed 30 simulation runs. The pdfs of the states were represented by 30.000 particles each.

Fig. 5(a) shows the agent position RMSEs obtained individually for the five trajectories versus time  $n$ , along with the overall RMSE averaged over the five trajectories. Fig. 5(b) shows the empirical cumulative distribution function (CDF) of the individual RMSEs and the empirical CDF of the five RMSEs taken together. It can be seen that the individual CDFs are very close to 1 already at RMSE equal to 0.12m or even less. The maximum of all the individual RMSEs is below 0.2m in all cases and below 0.083m in 90% of all cases.<sup>4</sup>

For an exemplary simulation run, Fig. 6 depicts the particles representing the posterior pdfs of the mobile agent and detected PF states as well as the MMSE position estimates of the detected PFs for the five trajectories. Almost all estimated PF positions can be associated with geometrically expected VA positions. This shows that the proposed algorithm is able to leverage position-related information contained in the radio signals for accurate and robust localization.

<sup>4</sup>The lower values of RMSE (below 0.072m in all cases and below 0.035m in 90% of all cases) obtained by the SLAM algorithm in [28] is due to an adaptive adjustment of the detection probability  $P_d$ .

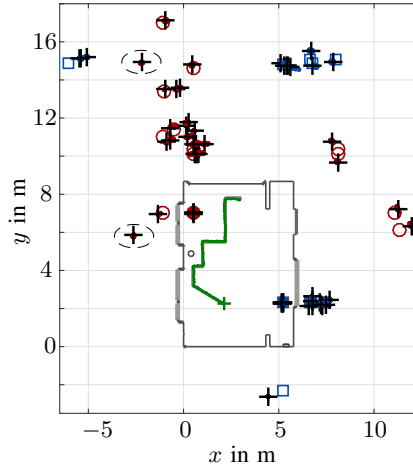


Fig. 6: Results for real measurements: Particles representing the posterior pdfs of the states of the detected PFs (red for PA 1, blue for PA 2). The positions of PA 1 and PA 2 are indicated by a red bullet and a blue box, respectively, and the corresponding geometrically expected VA positions by red circles and blue squares. The green line represents the MMSE estimates of the mobile agent position, and the green cross the MMSE estimate of the currently last mobile agent position. The black crosses indicate the MMSE estimates of the positions of the detected PFs. The dashed ellipses indicate PF positions that cannot be associated with geometrically expected VA positions.

### VIII. CONCLUSIONS AND FUTURE PERSPECTIVES

We proposed a radio signal based SLAM algorithm with probabilistic DA. The underlying system model describes specular MPCs in terms of VAs with unknown and possibly time-varying positions. A major complication in radio signal based SLAM is the DA problem, i.e., the unknown association of MPCs with VAs. To address this challenge, we modeled the entire SLAM problem including probabilistic DA in a Bayesian framework and represented the factorization of the joint posterior distribution by a factor graph. We then applied the BP scheme for approximate marginalization of the joint posterior distribution. This approach allowed the incorporation of an efficient BP algorithm for probabilistic DA that was originally proposed for multitarget tracking [36], [38]. Our factor graph extends that of [28] by the states of new potential features and undetected features. The intensity functions of the latter are tracked by a “zero-measurement” PHD filter, which improves the initialization of the positions of new potential features.

Simulation results using synthetic data showed that the proposed SLAM algorithm estimates the time-varying agent position and the feature map with high accuracy and robustness, even in conditions of strong clutter and low probability of detection. Moreover, an extensive experimental analysis using real ultra-wideband radio signals in an indoor environment showed that our algorithm performs similarly well in real-world scenarios; the agent position error was observed

to be below 0.2m for 100% and below 0.083m for 90% of all measurements.

A promising direction for future research is an extension of our algorithm that exploits further MPC parameters, such as AoAs and AoDs. Other possible extensions are to track additional types of features, such as scatter points, and to redefine the features to be extended objects. In the latter case, the BP-based DA needs to be adapted accordingly. Finally, operation in an unsynchronized sensor network and a distributed (decentralized) mode of operation would be theoretically and practically interesting. We also note that the complexity of our algorithm can be further reduced by using measurement gating and geometric data structures.

## REFERENCES

- [1] H. Durrant-Whyte and T. Bailey, "Simultaneous localization and mapping: Part I," *IEEE Robot. Autom. Mag.*, vol. 13, no. 2, pp. 99–110, Jun. 2006.
- [2] S. Thrun, W. Burgard, and D. Fox, *Probabilistic Robotics (Intelligent Robotics and Autonomous Agents)*. Cambridge, MA, USA: MIT Press, 2005.
- [3] R. Di Taranto, S. Muppirisetty, R. Raulefs, D. Slock, T. Svensson, and H. Wymeersch, "Location-aware communications for 5G networks: How location information can improve scalability, latency, and robustness of 5G," *IEEE Signal Process. Mag.*, vol. 31, no. 6, pp. 102–112, Nov 2014.
- [4] K. Witrals, P. Meissner, E. Leitinger, Y. Shen, C. Gustafson, F. Tufvesson, K. Haneda, D. Dardari, A. F. Molisch, A. Conti, and M. Z. Win, "High-accuracy localization for assisted living: 5G systems will turn multipath channels from foe to friend," *IEEE Signal Process. Mag.*, vol. 33, no. 2, pp. 59–70, Mar. 2016.
- [5] D. Dardari, P. Closas, and P. M. Djurić, "Indoor tracking: Theory, methods, and technologies," *IEEE Trans. Veh. Technol.*, vol. 64, no. 4, pp. 1263–1278, Apr. 2015.
- [6] F. Guidi, A. Guerra, and D. Dardari, "Personal mobile radars with millimeter-wave massive arrays for indoor mapping," *IEEE Trans. Mobile Comput.*, vol. 15, no. 6, pp. 1471–1484, Jun. 2016.
- [7] E. Leitinger, F. Meyer, P. Meissner, K. Witrals, and F. Hlawatsch, "Belief propagation based joint probabilistic data association for multipath-assisted indoor navigation and tracking," in *Proc. ICL-GNSS-16*, Barcelona, Spain, Jun. 2016.
- [8] H. Wymeersch, S. Marano, W. Gifford, and M. Win, "A machine learning approach to ranging error mitigation for UWB localization," *IEEE Trans. Commun.*, vol. 60, no. 6, pp. 1719–1728, Jun. 2012.
- [9] Y. Shen, S. Mazuelas, and M. Win, "Network Navigation: Theory and Interpretation," *IEEE J. Sel. Areas Commun.*, vol. 30, no. 9, pp. 1823–1834, Oct. 2012.
- [10] C. Gentner, T. Jost, W. Wang, S. Zhang, A. Dammann, and U. C. Fiebig, "Multipath assisted positioning with simultaneous localization and mapping," *IEEE Trans. Wireless Commun.*, vol. 15, no. 9, pp. 6104–6117, Sep. 2016.
- [11] E. Leitinger, P. Meissner, C. Rudisser, G. Dumhart, and K. Witrals, "Evaluation of position-related information in multipath components for indoor positioning," *IEEE J. Sel. Areas Commun.*, vol. 33, no. 11, pp. 2313–2328, Nov. 2015.
- [12] J. Borish, "Extension of the image model to arbitrary polyhedra," *The Journal of the Acoustical Society of America*, Mar. 1984.
- [13] M. Dissanayake, P. Newman, S. Clark, H. Durrant-Whyte, and M. Csorba, "A solution to the simultaneous localization and map building (SLAM) problem," *IEEE Trans. Robot. Autom.*, vol. 17, no. 3, pp. 229–241, Jun. 2001.

- [14] J. Mullane, B.-N. Vo, M. Adams, and B.-T. Vo, "A random-finite-set approach to Bayesian SLAM," *IEEE Trans. Robot.*, vol. 27, no. 2, pp. 268–282, Apr. 2011.
- [15] M. Montemerlo and S. Thrun, "Simultaneous localization and mapping with unknown data association using FastSLAM," in *2003 IEEE International Conference on Robotics and Automation*, vol. 2, Sept 2003, pp. 1985–1991 vol.2.
- [16] M. Lundgren, L. Svensson, and L. Hammarstrand, "Variational Bayesian expectation maximization for radar map estimation," *IEEE Trans. Signal Process.*, vol. 64, no. 6, pp. 1391–1404, Mar. 2016.
- [17] M. Fatemi, L. Svensson, L. Hammarstrand, and M. Lundgren, "Variational Bayesian EM for SLAM," in *Proc. IEEE CAMSAP-15*, Cancun, Mexico, Dec. 2015, pp. 501–504.
- [18] H. Deusch, S. Reuter, and K. Dietmayer, "The labeled multi-Bernoulli SLAM filter," *IEEE Signal Process. Lett.*, vol. 22, no. 10, pp. 1561–1565, Oct. 2015.
- [19] M. Fatemi, K. Granström, L. Svensson, F. J. R. Ruiz, and L. Hammarstrand, "Poisson multi-Bernoulli mapping using Gibbs sampling," *IEEE Trans. Signal Process.*, vol. 65, no. 11, pp. 2814–2827, Jun. 2017.
- [20] E. Leitinger, P. Meissner, M. Lafer, and K. Witrisal, "Simultaneous localization and mapping using multipath channel information," in *Proc. IEEE ICCW-15*, London, UK, Jun. 2015, pp. 754–760.
- [21] M. Zhu, J. Vieira, Y. Kuang, K. Astrom, A. Molisch, and F. Tufvesson, "Tracking and positioning using phase information from estimated multi-path components," in *Proc. IEEE ICCW-15*, London, UK, Jun. 2015, pp. 712–717.
- [22] B. Fleury, M. Tschudin, R. Heddergott, D. Dahlhaus, and K. Ingeman Pedersen, "Channel parameter estimation in mobile radio environments using the SAGE algorithm," *IEEE J. Sel. Areas Commun.*, vol. 17, no. 3, pp. 434–450, Mar. 1999.
- [23] A. Richter, "Estimation of Radio Channel Parameters," Ph.D. dissertation, Ilmenau University of Technology, 2005.
- [24] J. Salmi and A. Molisch, "Propagation parameter estimation, modeling and measurements for ultrawideband MIMO radar," *IEEE Trans. Antennas Propag.*, vol. 59, no. 11, pp. 4257–4267, Nov. 2011.
- [25] D. Shutin, W. Wang, and T. Jost, "Incremental sparse Bayesian learning for parameter estimation of superimposed signals," in *Proc. SampTA-13*, Bremen, Germany, Jul. 2013.
- [26] M. A. Badiu, T. L. Hansen, and B. H. Fleury, "Variational Bayesian inference of line spectra," *IEEE Trans. Signal Process.*, vol. 65, no. 9, pp. 2247–2261, May 2017.
- [27] B. Etlzinger, F. Meyer, F. Hlawatsch, A. Springer, and H. Wymeersch, "Cooperative simultaneous localization and synchronization in mobile agent networks," *IEEE Trans. Signal Process.*, vol. 65, no. 14, pp. 3587–3602, Jul. 2017.
- [28] E. Leitinger, F. Meyer, F. Tufvesson, and K. Witrisal, "Factor graph based simultaneous localization and mapping using multipath channel information," in *Proc. IEEE ICC-17*, Paris, France, Jun. 2017.
- [29] Y. Bar-Shalom and X.-R. Li, *Multitarget-Multisensor Tracking: Principles and Techniques*. Storrs, CT, USA: Yaakov Bar-Shalom, 1995.
- [30] D. Musicki and R. Evans, "Joint integrated probabilistic data association: JIPDA," *IEEE Trans. Aerosp. Electron. Syst.*, vol. 40, no. 3, pp. 1093–1099, Jul. 2004.
- [31] P. Horridge and S. Maskell, "Searching for, initiating and tracking multiple targets using existence probabilities," in *Proc. FUSION-09*, Seattle, WA, USA, Jul. 2009, pp. 611–617.
- [32] —, "Using a probabilistic hypothesis density filter to confirm tracks in a multi-target environment," in *Proc. INFORMATIK-11*, Berlin, Germany, Jul. 2011.
- [33] R. P. S. Mahler, *Statistical Multisource-Multitarget Information Fusion*. Norwood, MA, USA: Artech House, 2007.
- [34] H.-A. Loeliger, "An introduction to factor graphs," *IEEE Signal Process. Mag.*, vol. 21, no. 1, pp. 28–41, Jan. 2004.
- [35] F. Kschischang, B. Frey, and H.-A. Loeliger, "Factor graphs and the sum-product algorithm," *IEEE Trans. Inf. Theory*, vol. 47, no. 2, pp. 498–519, Feb. 2001.

- [36] J. Williams and R. Lau, "Approximate evaluation of marginal association probabilities with belief propagation," *IEEE Trans. Aerosp. Electron. Syst.*, vol. 50, no. 4, pp. 2942–2959, Oct. 2014.
- [37] F. Meyer, T. Kropfreiter, J. L. Williams, R. A. Lau, F. Hlawatsch, P. Braca, and M. Z. Win, "Message passing algorithms for scalable multitarget tracking," *Proc. IEEE*, vol. 106, no. 2, pp. 221–259, Feb. 2018.
- [38] F. Meyer, P. Braca, P. Willett, and F. Hlawatsch, "A scalable algorithm for tracking an unknown number of targets using multiple sensors," *IEEE Trans. Signal Process.*, vol. 65, no. 13, pp. 3478–3493, Jul. 2017.
- [39] F. Meyer, P. Braca, F. Hlawatsch, M. Micheli, and K. LePage, "Scalable adaptive multitarget tracking using multiple sensors," in *Proc. IEEE GLOBECOM-16*, Washington D.C., USA, Dec. 2016.
- [40] F. Meyer, P. Braca, P. Willett, and F. Hlawatsch, "Tracking an unknown number of targets using multiple sensors: A belief propagation method," in *Proc. FUSION-16*, Heidelberg, Germany, Jul. 2016, pp. 719–726.
- [41] —, "Scalable Multitarget Tracking using Multiple Sensors: A belief propagation approach," in *Proc. FUSION-15*, Jul. 2015, pp. 1778–1785.
- [42] J. L. Williams, "Marginal multi-Bernoulli filters: RFS derivation of MHT, JIPDA, and association-based MeMBer," *IEEE Trans. Aerosp. Electron. Syst.*, vol. 51, no. 3, pp. 1664–1687, Jul. 2015.
- [43] T. Kropfreiter, F. Meyer, and F. Hlawatsch, "Sequential Monte Carlo implementation of the track-oriented marginal multi-Bernoulli/Poisson filter," in *Proc. FUSION-16*, Heidelberg, Germany, Jul. 2016, pp. 972–979.
- [44] A. D. Marrs, "Asynchronous multi-sensor tracking in clutter with uncertain sensor locations using Bayesian sequential Monte Carlo methods," in *IEEE Proc. Aerosp.*, vol. 5, March 2001, pp. 2171–2178.
- [45] E. Leitinger, S. Grebien, X. Li, F. Tufvesson, and K. Witrisal, "On the use of MPC amplitude information in radio signal based SLAM," in *IEEE SSP 2018*, Freiburg im Breisgau, Germany, Jun. 2018.
- [46] T. Jost, W. Wang, U. Fiebig, and F. Perez-Fontan, "Detection and tracking of mobile propagation channel paths," *IEEE Trans. Antennas Propag.*, vol. 60, no. 10, pp. 4875–4883, Oct. 2012.
- [47] J. Vermaak, S. J. Godsill, and P. Perez, "Monte Carlo filtering for multi target tracking and data association," *IEEE Trans. Aerosp. Electron. Syst.*, vol. 41, no. 1, pp. 309–332, Jan. 2005.
- [48] S. Kay, *Fundamentals of Statistical Signal Processing: Estimation Theory*. Upper Saddle River, NJ, USA: Prentice Hall, 1993.
- [49] F. Meyer, O. Hlinka, H. Wymeersch, E. Riegler, and F. Hlawatsch, "Distributed localization and tracking of mobile networks including noncooperative objects," *IEEE Trans. Signal Inf. Process. Netw.*, vol. 2, no. 1, pp. 57–71, Mar. 2016.
- [50] D. J. Daley and D. Vere-Jones, *An Introduction to the Theory of Point Processes. Vol. I*, 2nd ed. New York, NY, USA: Springer, 2003.
- [51] Y. Bar-Shalom, T. Kirubarajan, and X.-R. Li, *Estimation with Applications to Tracking and Navigation*. New York, NY, USA: Wiley, 2002.
- [52] D. Schuhmacher, B.-T. Vo, and B.-N. Vo, "A consistent metric for performance evaluation of multi-object filters," *IEEE Trans. Signal Process.*, vol. 56, no. 8, pp. 3447–3457, Aug. 2008.
- [53] A. S. Rahmathullah, Á. F. García-Fernández, and L. Svensson, "Generalized optimal sub-pattern assignment metric," in *Proc. FUSION-17*, Jul. 2017, pp. 1–8.
- [54] J. Neira and J. D. Tardos, "Data association in stochastic mapping using the joint compatibility test," *IEEE Transactions on Robotics and Automation*, vol. 17, no. 6, pp. 890–897, Dec. 2001.
- [55] P. Meissner, E. Leitinger, and K. Witrisal, "UWB for robust indoor tracking: Weighting of multipath components for efficient estimation," *IEEE Wireless Comm. Lett.*, vol. 3, no. 5, pp. 501–504, Oct. 2014.